International Journal of Mathematical, Engineering and Management Sciences
Vol. 11, No. 1, 376-399 2026
https://doi.org/10.33889/IJMEMS.2026.11.1.016

A New Approximate Analytical Method and its Convergence for Fuzzy Time-Fractional Advection-Diffusion Equations

Manju Kashyap
Department of Applied Sciences and Humanities,
Galgotias College of Engineering and Technology, Greater Noida, India.
E-mail: drmanju.kashyap@galgotiacollege.edu

Surbhi Gupta
Department of Mathematics,
Amity University, Noida, India.
Corresponding author: sgupta11@amity.edu

Nahid Fatima
Department of Mathematics and Sciences,
Prince Sultan University Riyadh, Saudi Arabia.
E-mail: drnahidfatima@gmail.com, nfatima@psu.edu.sa

(Received on June 30, 2025; Revised on September 17, 2025 & November 20, 2025; Accepted on November 25, 2025)

Abstract
This article introduces a new numerical approach based on the Laplace Homotopy Perturbation Method (LHPM) to solve the one-dimensional Fuzzy Time-Fractional Advection-Diffusion Equation (FTFADE) in the Caputo sense, considering fuzzy initial conditions. The proposed method demonstrates how fuzzy numerical solutions gradually converge to precise ones, supported by clear illustrative examples. We also establish sufficient conditions that guarantee the uniqueness of the solution and analyze the convergence of the method. Moreover, we compare fuzzy solutions for different uncertainty levels and fractional orders to provide a deeper understanding of the model's behavior. The results are presented graphically to highlight the accuracy, efficiency, and reliability of the proposed method.

Keywords- Caputo fractional derivative, Fuzzy fractional partial differential equation, Perturbation, Homotopy, Advection diffusion equation.

1. Introduction

The investigation of Fuzzy Fractional Partial Differential Equation (FFPDE) has garnered significant interest from numerous researchers and emerged as a prominent focus within uncertain mathematical analysis. Fractional order models of fuzzy differential equations hold greater significance compared to their conventional integer-order models. The research on the theory of Fractional Partial Differential Equation (FPDE) of non-integer order is interesting due to these theories provides an effective approach for recitation uncertainty that manifests in several fields of dynamical systems affected by roughness and exhibiting non-standard dynamical behaviours with hereditary effects. Also, studies on the numerical solutions of fractional PDE have been increasing in number along with the development of fuzzy fractional calculus. PDEs play a vital role in numerous engineering applications, plasma physics, and various branches of science, as anticipated in forthcoming studies (Dumbser et al., 2023). The Advection Diffusion Equation (ADE)is extensively utilized across multiple domains of science and engineering, encompassing atmospheric science, environmental science application (Zhang et al., 2022). The ADE, Partial Differential Equation (PDE), arises in many physicaland engineering applications, such as porous media flow (Nikan et al., 2020), groundwater hydrology (Rahaman et al., 2022), and chemical

engineering, where the transport of solutes or contaminants is influenced by both advection and diffusion. ADE finds crucial applications in modelling the transportation of air pollutants and water pollutants within the atmosphere and water bodies, carrying significant implications for public health and the environment. This is important for understanding the fate of pollutants and assessing the potential impact on aquatic ecosystems and human health (Singh et al., 2019) Therefore fuzzy and fractional form of advection diffusion equation will be a potent tool for comprehending the movement of substances in various physical and biological systems. The Time-Fractional ADE (TFADE), which extends the conventional ADE by integrating fractional time derivatives, has grown in popularity in recent years (Zhang et al., 2022; Shah et al., 2023).

Fractional calculus has proven to be a valuable tool for modeling anomalous diffusion phenomena, which classical diffusion models cannot sufficiently describe. Many FPDE are used in the study of numerical simulations and analytical approaches for magneto-acoustic waves in cold plasma. The wide application of fractional calculus results in plenty of books, and research articles. It is significantly playing a vital role in science, technology, engineering, and biological problems of the real-world (Podlubny, 1998; Petrá, 2011). Over the last two decades, researchers have become increasingly interested in exploring analytical and approximate solutions for FPDEs in initial and boundary situations (Rezazadeh et al., 2019; Zafar et al., 2022). PDEs and FPDEs have been solved numerically using various methods, such asVariational Iteration Method (VIM), Homotopy Analysis Method (HAM), Adomian Decomposition Method(ADM), Transform, finite difference, neural networks method (Shah et al., 2025a, 2025b), wavelet technique (Jahan et al., 2025), new extended direct algebraic method (Rezazadeh, 2018) etc., depending on the specific problem and boundary conditions. Remarkably, these established techniques for non-linear and linear Fractional Differential Equation (FDE) and FPDE have demonstrated reliability and efficiency in providing analytical and numerical solutions for real-world problems. While many physical phenomena depend on both space and time, FPDE can take account of time and space aspects by incorporating vivid fractional derivative operators (Karniadakis et al., 2015; Bilal et al., 2024). In Eslami & Rezazadeh (2016) integral technique for analytic solution of nonlinear conformable time-fractional partial differential equations. Besides, the fractional differential operator offers a higher degree of flexibility in solving complex problems. The theories of Riemann-Liouville, Hadamard, Caputo, Caputo-Hadamard fractional integral or derivative operators, Cuputo Fabrizio have been used for a great deal in many manuscripts. Among various fractional differential operators Caputo, a useful operator, provides a greater degree of freedom. As a result, this area has received a lot of interest, and several research articles, monographs, books, etc. have been written about it from various angles on various fractional problems (Kumar et al., 2017, Rubbab et al., 2021, Ahmad et al., 2025).

One more concept, that is, concept of fuzzy (Zadeh, 1965) is often used in the context of complex systems, where traditional methods of modeling and analysis may not be sufficient to accurately represent the behaviour of the system. Over the recent years, several applications of theory of fuzzy set in research have witnessed a surge, encompassing the concepts of fixed-point, control systems, topology, fuzzy automata, and other areas. Chang & Zadeh (1996) expanded the theory of fuzzy sets by introducing fuzzy control and mapping. The idea of "fuzzy time" pertains to time being treated as a fuzzy variable, implying that it lacks precise definition and carries some degree of uncertainty. Fuzzy numbers, as compared with crisp numbers, have been employed to represent the parameters in situations where the information appears fuzzy and insufficient. Fuzzy differential, partial and integral equations have garnered significant attention from researchers in applied sciences (Babolian et al., 2004; Salahshour et al., 2012a; Chakraverty et al., 2016). Subsequently, the mathematical modeling of specific real-world systems, accounting for data uncertainty, has led to the emergence of FFADE. Over the past decade, a large number of researchers have shown interest in the model of fuzzy and fractional together (Salahshour et

al., 2012a; Tapaswini & Chakraverty, 2013). The upper and lower solution method, as well as the monotone iterative strategy, were described by the authors (Alikhani & Bahrami, 2013) as ways to find maximal and minimal solutions for the fuzzy fractional integrodifferential equations. In recent years, numerous scholars have delved into the FFPDE using various models, leading to significant contributions from researchers such as (Ahmadian et al., 2018; Allahviranloo & Ghanbari, 2020; Zureigat et al., 2021). Researchers Shah et al. (2020), Ahmad et al. (2021) and Pedro et al. (2023) have utilized effective mathematical technique numerical analytical methods to FFPDE. Notably, (Naeem et al., 2022) have conferred applications of derivative for solving fuzzy fractional order KdV equation. Furthermore, as demonstrated by Hoa et al. (2019), and Vu et al. (2022), authors have investigated new techniques for finding the solutions of CK fuzzy FDE. Keshavarz et al. (2022) solved a fuzzy fractional diffusion model of cancer tumours using fuzzy integral transforms. The FTFADE holds significant potential for application in the realm of environmental engineering, specifically in the study of groundwater contamination. The incorporation of fuzzy time aspect in the equation enables more realistic modeling of the unpredictable nature of groundwater flow and contaminant transport over time (Li et al., 2020). Authors (Kirtiwant et al., 2017; Li et al., 2019; Aghdam et al., 2021; Zureigat et al., 2021; Zhang et al., 2022) have applied various methods, depending on the FTFAD problem with initial and boundary condition.

It appears that only an insignificant amount of study physicalhas been using Homotopy Perturbation Method (HPM)coupled with Laplace transform (LHPM) on FFADE. LHPM is a powerful numerical technique that synergizes the Laplace transform and the HPM. In situations where, conventional analytical methods fall short in solving nonlinear differential equations, the LHPM proves to be a valuable tool. Its versatility makes it a valuable tool in diverse scientific and engineering domains that frequently encounter nonlinear problems. He (1999) was the first to propose the HPM. Since then, many authors have studied and applied this method on linear and nonlinear PDE in a variety of scientific as well technological disciplines. The HPM (He, 2005; Tapaswini & Chakraverty, 2013), ADM (Duan et al., 2012), VIM (Ganji, 2012), LHPM (Kashyap et al., 2023; Kashyap et al., 2025) have all found applications in studying diverse physical problems. The motivation behind this work is to discuss comparative analysis of proposed method on FTFADE at different fractional orders and various uncertainty level r. LHPM has been successfully employed in handling linear, nonlinear differential equations, PDEs, and fractional PDE resulting in more accurate outcomes as related to methods. Moreover, we conduct a comparative analysis among approximate solutions for FTFADE at various fractional orders ranging from 0 to 1 in the Caputo sense. The LHPM scheme is utilized, and its performance is compared with the exact solutions of test cases to assess its accuracy and effectiveness.

The structure of paper is summarized as: in Section 2 we discuss a review of theorems and lemmas. Section 3 exhibits a discussion of FTFADE, while Section 4 discusses about uniqueness and convergence of LHPM solution on FTFADE. In the next Section 5 proposed method on FTFADE. Moving on to Section 6, the proposed method is validated through the utilization of two cases. Section 7 with subsection presents a thorough analysis of the outcomes of FTFADE, utilizing numerical approximations, graphs, and tables, numerical comparison and validation, sensitivity analysis of fuzzy parameters and comparative analysis with existing methods. Finally, Section 8 contains the conclusion of this paper and discusses the outlines potential future developments.

2. Preliminaries

This section provides some notations and definitions, which we have referenced later in this paper. It also presents the concept of fuzzy numbers, with various theorems defined in references (Dubois & Prade, 1982; Salahshour et al., 2012a; El Mfadel et al., 2021).

***Definition* 2.1** Fuzzy number (Tapaswini & Chakraverty, 2013)
A fuzzy number w is convex normalized fuzzy set $\widetilde{w}$ of the real line R such that
$\{\mu_{\widetilde{w}}(\mathcal{X})\colon R \to [0,1], \forall\, \mathcal{X} \in R\}$Where $\mu_{\widetilde{w}}$ is called the membership function of the fuzzy set and it is piecewise continuous.

***Definition* 2.2** Triangular fuzzy number (TFN) (Tapaswini & Chakraverty, 2013)
TFN represented by $\widetilde{w}$ can be defined as convex and normalized fuzzy set $\widetilde{U}$ on the real number line R. This definition encompasses the following key characteristics.
i) $\mathcal{X}_0 \in R$ for which $\mu_{\widetilde{w}}(\mathcal{X}_0) = 1(\mathcal{X}_0$ is designated as mean value of $\widetilde{w})$, where $\mu_{\widetilde{w}}$ is called the membership function of the fuzzy set.
ii) $\mu_{\widetilde{w}}(\mathcal{X})$ is piecewise continuous.

***Definition* 2.3** In parametric form (Shah et al., 2020), the fuzzy number can be represented as
$\tilde{k}(r) = \left[\underline{k}(r), \bar{k}(r)\right]$ where $r \in [0, 1]$ satisfies the following conditions:
i) $\underline{k}(r)$ is left side continuous, bounded, and increasing function.
ii) $\bar{k}(r)$ is right side continuous, bounded and decreasing function.
iii) $\underline{k}(r) \leq \bar{k}(r)$.
where, r is a crisp number "if $\underline{k}(r) = \overline{k}(r) = r$.

***Definition* 2.4** A continuous fuzzy function $\widetilde{w}$ on $[0, b] \subset R$ (Shah et al., 2020), then fuzzy fractional integral in Riemann-Liouvilli sense corresponding to t as
$I^{\theta}\widetilde{w}(t) = \int_0^t \frac{(t-\Omega)^{\theta-1}\widetilde{w}(\Omega)}{\Gamma(\Omega)}\, d\Omega,\ \ \Omega \in (0, \infty)$.

As $\widetilde{w} \in C^F[0, b] \cap L^F[0, b]$, where, $C^F[0, b]$ is the space of fuzzy continuous functions and $L^F[0, b]$ is the space of fuzzy Lebesgue integrable functions respectively, then fractional fuzzy integral is defined as:
$[I^{\theta}\widetilde{w}(t)]_r = \left[I^{\theta}\underline{w_r}(t), I^{\theta}\overline{w}_r(t)\right], 0 \leq r \leq 1$ such that

$$I^{\theta}\underline{w_r}(t) = \int_0^t \frac{(t-\Omega)^{\theta-1}\underline{w}(\Omega)}{\Gamma(\Omega)}\, d\Omega,$$

$$\theta\,, \Omega\ \in (0, \infty).$$

$$I^{\theta}\overline{w}_r(t) = \int_0^t \frac{(t-\Omega)^{\theta-1}\overline{w}(\Omega)}{\Gamma(\Omega)}\, d\Omega,$$

$$\theta\,, \Omega\ \in (0, \infty).$$

***Definition* 2.5** A function $\widetilde{w} \in C^F[0, b] \cap L^F[0, b]$ (Shah et al., 2020, Arfan et al., 2021), Caputo fractional derivative is defined as $[D^{\theta}\widetilde{w}(t)]_r = \left[D^{\theta}\underline{w_r}(t), D^{\theta}\overline{w}_r(t)\right],\ 0 \leq r \leq 1$, where

$$D^{\theta}\underline{w_r}(t) = \left[\int_0^t \frac{(t-\Omega)^{m-\theta-1}\frac{d^m}{d\Omega^m}\underline{w}(\Omega)}{\Gamma(m-\xi)}\, d\xi\ \right]_{t=t_0},$$

$$D^{\theta}\overline{w_r}(t) = \left[\int_0^t \frac{(t-\Omega)^{m-\theta-1}\frac{d^m}{d\Omega^m}\overline{w}(\Omega)}{\Gamma(m-\Omega)}\, d\Omega\ \right]_{t=t_0}.$$

such that the integration on right sides converges and $m = [\theta]$.

***Definition* 2.6** Let $\widetilde{w} \in C^F[0,b] \cap L^F[0,b]$ such that $[\widetilde{w}(t)]_r = \left[\underline{w_r}(t), \overline{w}_r(t)\right]$ where, $0 \le r \le 1$.The Laplace transform of fuzzy Caputo derivative of order $0 < \alpha \le 1$ is defined as (Salahshour et al., 2012a):

$$L\left(D_t{}^{\alpha}\widetilde{w_r}(t)\right) = \left[\, L\left(D_t{}^{\alpha}\underline{w_r}(t)\right), L\left(D_t{}^{\alpha}\overline{w_r}(t)\right)\right].$$

where,

$$\left[\, L\left(D_t{}^{\alpha}\underline{w_r}(t)\right)\right] = s^{\alpha}L\left(\underline{w_r}(t)\right) - s^{\alpha-1}\underline{w_r}(0), \text{ and}$$

$$\left[\, L\left(D_t{}^{\alpha}\overline{w_r}(t)\right)\right] = s^{\alpha}L\left(\overline{w_r}(t)\right) - s^{\alpha-1}\overline{w_r}(0).$$

3. Fuzzy Time-Fractional Advection-Diffusion Equation (FTFADE)

The focal point of this investigation is the time fractional one-dimensional ADE as introduced by Zureigat et al. (2021). FTFADE is an effective tool for comprehending and simulating transport phenomena in systems with uncertain, nonlocal, and memory-driven behaviours. In this equation, the Caputo fractional derivative is employed, giving rise to the one-dimensional FTFADE. To elaborate further, the representation of the FTFADE is provided below:

$$D_t{}^{\alpha}\tilde{u}(\mathcal{X},\mathrm{t}) = \tilde{a}(\mathcal{X})\, D_{\mathcal{X}}\tilde{u}(\mathcal{X},t) + \tilde{b}(\mathcal{X})D_{\mathcal{X}\mathcal{X}}\tilde{u}(\mathcal{X},t) + \tilde{q}(\mathcal{X},t), \quad 0 < \alpha \le 1 \tag{1}$$

with fuzziness in the initial and boundary conditions

$$\tilde{u}(\mathcal{X},0) = \tilde{g}(\mathcal{X}), \quad 0 < \mathcal{X} \le l \tag{2}$$

$$\tilde{u}(0,t) = \tilde{f}_0(\mathcal{X}), \tilde{u}(l,t) = \tilde{f}_1(t), \quad t > 0 \tag{3}$$

Equation (1) defines the fuzzy concentration, denoted as $\tilde{u}(\mathcal{X},t)$ which represents a quantity, such as mass and energy, with respect to precise variables $\mathcal{X}$ and t. It incorporates the fuzzy time fractional derivative $D_t{}^{\alpha}$ of order α. The parameters $\tilde{a}(\mathcal{X})$, $\tilde{b}(\mathcal{X})$ and $\tilde{q}(\mathcal{X},t) = \tilde{k}(r)\, q(\mathcal{X},t)$ are the average velocity, diffusion coefficient, and fuzzy function of crisp variables, respectively.

The fuzzy initial condition and boundary conditions are expressed as $\tilde{u}(\mathcal{X},0)$, $\tilde{u}(0,t)$, and $\tilde{u}(l,t)$ respectively. Now, when Equation (1) is formulated in terms of the r - level (uncertainty level), it results in the following representation.

$$\left[D_t{}^{\alpha}\underline{u}(\mathcal{X},t{:}\,r), D_t{}^{\alpha}\overline{u}(\mathcal{X},t{:}\,r)\right] = \left[\underline{a}(\mathcal{X}{:}\,r), \overline{a}(\mathcal{X}{:}\,r)\right]\left[D_{\mathcal{X}}\underline{u}(\mathcal{X},t{:}\,r), D_{\mathcal{X}}\overline{u}(\mathcal{X},t{:}\,r)\right] +$$

$$\left[\underline{b}(\mathcal{X}{:}\,r), \overline{b}(\mathcal{X}{:}\,r)\right]\left[D_{xx}\underline{u}(\mathcal{X},t{:}\,r), D_{\mathcal{X}\mathcal{X}}\overline{u}(\mathcal{X},t{:}\,r)\right] + \left[\underline{q}(\mathcal{X},t{:}\,r), \overline{q}(\mathcal{X},t{:}\,r)\right] \tag{4}$$

Given the uncertain initial condition, the equation can be expressed with the following notation:

$$\left[\underline{u}(\mathcal{X},0{:}\,r), \overline{u}(\mathcal{X},0{:}\,r)\right] = \left[\underline{g}(\mathcal{X},0{:}\,r), \overline{g}(\mathcal{X},0{:}\,r)\right] \tag{5}$$

and the accompanying boundary conditions are outlined below.

$$\left[\underline{u}(0,t{:}\,r), \overline{u}(0,t{:}\,r)\right] = \left[\underline{f_0}(\mathcal{X},0{:}\,r), \overline{f_0}(\mathcal{X},0{:}\,r)\right] \tag{6}$$

$$\left[\underline{u}(l,t{:}\,r), \overline{u}(l,t{:}\,r)\right] = \left[\underline{f_1}(l,t{:}\,r), \overline{f_1}(l,t{:}\,r)\right] \tag{7}$$

4. Analysis of Uniqueness and Convergence in FTFADE Solution

In this section, we discuss the uniqueness and convergence of the LHPM solution for the FTFADE:

Theorem 1 (Uniqueness Theorem): The LHPM solution of FTFADE is unique, whenever $0 < \beta < 1$, where, $\beta = \{\tilde{a}(\mathcal{X})\delta + \tilde{b}(\mathcal{X})\sigma\}$ T.

***Proof*:** The solution of FTFADE in Equation (1) is $\tilde{u}(\mathcal{X},t) = \sum_{n=0}^{\infty} u_n(\mathcal{X},t)$. Assuming $\tilde{u}$ and $\tilde{u}^*$ be two different solutions of FTFADE (1) such that $|\tilde{u}| \leq$ A and $|\tilde{u}^*| \leq$ B. Now we have

$$|\tilde{u} - \tilde{u}^*| = \left| L^{-1}\left[\frac{1}{s^\alpha} \mathrm{L}\left[\tilde{a}(\mathcal{X})\mathrm{D}_{\mathcal{X}}(\tilde{u} - \tilde{u}^*) + \tilde{b}(\mathcal{X})\mathrm{D}_{\mathcal{X}\mathcal{X}}(\tilde{u} - \tilde{u}^*)\right]\right]\right|,$$

Applying the convolution theorem to the inverse Laplace Transform yields the following outcome:

$$\left| L^{-1}\left[\frac{1}{s^\alpha} \mathrm{L}\left[\tilde{a}(\mathcal{X})\mathrm{D}_{\mathcal{X}}(\tilde{u} - \tilde{u}^*) + \tilde{b}(\mathcal{X})\mathrm{D}_{\mathcal{X}\mathcal{X}}(\tilde{u} - \tilde{u}^*)\right]\right]\right|$$

$$= \left| \int_0^t \left\{\tilde{a}(\mathcal{X})\mathrm{D}_{\mathcal{X}}(\tilde{u} - \tilde{u}^*) + \tilde{b}(\mathcal{X})\mathrm{D}_{\mathcal{X}\mathcal{X}}(\tilde{u} - \tilde{u}^*)\right\} \frac{(t-\xi)^\alpha}{\Gamma(1+\alpha)} \, \mathrm{d}\,\xi \right|,$$

$$\leq \int_0^t \left| \left\{\tilde{a}(\mathcal{X})\mathrm{D}_{\mathcal{X}}(\tilde{u} - \tilde{u}^*) + \tilde{b}(\mathcal{X})\mathrm{D}_{\mathcal{X}\mathcal{X}}(\tilde{u} - \tilde{u}^*)\right\} \frac{(t-\xi)^\alpha}{\Gamma(1+\alpha)} \, \mathrm{d}\xi \right|,$$

$$\leq \tilde{a}(\mathcal{X}) \int_0^t \mathrm{D}_{\mathcal{X}}(|\tilde{u} - \tilde{u}^*|) + \tilde{b}(\mathcal{X}) \int_0^t \mathrm{D}_{\mathcal{X}\mathcal{X}}(|\tilde{u} - \tilde{u}^*|) \frac{(t-\xi)^\alpha}{\Gamma(1+\alpha)} \, \mathrm{d}\xi,$$

$$\leq \left\{\tilde{a}(\mathcal{X}) \int_0^t \delta(|\tilde{u} - \tilde{u}^*|) + \tilde{b}(\mathcal{X}) \int_0^t \sigma(|\tilde{u} - \tilde{u}^*|)\right\} \frac{(t-\xi)^\alpha}{\Gamma(1+\alpha)} \, \mathrm{d}\xi.$$

Utilizing the integral mean value theorem on the equation above, we obtain the following result:

$$\leq \{\tilde{a}(\mathcal{X})\delta(|\tilde{u} - \tilde{u}^*|) + \tilde{b}(\mathcal{X})\sigma(|\tilde{u} - \tilde{u}^*|)\} \text{ T},$$

$$\leq (|\tilde{u} - \tilde{u}^*|)\{\tilde{a}(\mathcal{X})\delta + \tilde{b}(\mathcal{X})\sigma\},$$

$$\leq \beta|\tilde{u} - \tilde{u}^*|,$$

Further it gives $|\tilde{u} - \tilde{u}^*|\,(1-\beta) \leq 0$, as $0 < \beta < 1$.

Hence $|\tilde{u} - \tilde{u}^*| = 0$ and so $\tilde{u} = \tilde{u}^*$. Therefore, the LHPM solution is unique.

Theorem 2 (Convergence Theorem) (Salahshour et al., 2012b; Kumar et al., 2018; Verma et al., 2023): Let E be a Banach space. Then there exists a nonlinear mapping defined from $\mathrm{F}: \mathrm{E} \to \mathrm{E}$, such that $\|\mathrm{F}(\tilde{u}) - \mathrm{F}(\tilde{\mu})\| \leq \beta\|\tilde{u} - \tilde{\mu}\|$, $\forall u, \mu \epsilon$ E. According to Banach's fixed point theory, F has a fixed point, and if $\tilde{u}_0,\ \tilde{\mu}_0 \epsilon$ E then the sequence formed by the LHPM solution converges to the fixed-point F.

$$\|\tilde{u}_m - \tilde{u}_n\| \leq \frac{\beta^n}{(1-\beta)}\|\tilde{u}_1 - u_0\|.$$

***Proof*:** Let Banach space $(\mathrm{C}[\mathrm{J}], \|.\|)$ of all the continuous functions on J with the norm defined as $\|g(\mathrm{t})\| = \max_{\mathrm{t}\epsilon\mathrm{J}}|g(t)|$.

Consider $\|\tilde{u}_m - \tilde{u}_n\| = max_{\,t\epsilon J}|\tilde{u}_m - \tilde{u}_n|$,

$$= max_{\,t\epsilon J} \left| L^{-1}\left[\frac{1}{s^\alpha} L\left[\tilde{a}(\mathcal{X})D_{\mathcal{X}}(\tilde{u}_{m-1} - \tilde{u}_{n-1}) + \tilde{b}(\mathcal{X})D_{\mathcal{X}\mathcal{X}}(\tilde{u}_{m-1} - \tilde{u}_{n-1})\right]\right]\right|.$$

Applying the convolution theorem to the inverse Laplace Transform, the subsequent outcome is as follows:

$$= \max_{t\epsilon J} \left| \int_0^t \{\tilde{a}(X) D_X(\tilde{u}_{m-1} - \tilde{u}_{n-1}) + \tilde{b}(X) D_{XX}(\tilde{u}_{m-1} - \tilde{u}_{n-1})\} \frac{(t-\xi)^\alpha}{\Gamma(1+\alpha)} \, d\xi \right|,$$

$$\leq \max_{t\epsilon J} \int_0^t \left| \{\tilde{a}(X) D_X(\tilde{u}_{m-1} - \tilde{u}_{n-1}) + \tilde{b}(X) D_{XX}(\tilde{u}_{m-1} - \tilde{u}_{n-1})\} \frac{(t-\xi)^\alpha}{\Gamma(1+\alpha)} \, d\xi \right|,$$

$$\leq \max_{t\epsilon J} \left\{ \tilde{a}(X) \int_0^t D_X(|\tilde{u}_{m-1} - \tilde{u}_{n-1}|) + \tilde{b}(X) \int_0^t D_{XX}(|\tilde{u}_{m-1} - \tilde{u}_{n-1}|) \right\} \frac{(t-\xi)^\alpha}{\Gamma(1+\alpha)} \, d\xi \,,$$

$$\leq \max_{t\epsilon J} \left\{ \tilde{a}(X) \int_0^t \delta(|\tilde{u}_{m-1} - \tilde{u}_{n-1}|) + \tilde{b}(X) \int_0^t \sigma(|\tilde{u}_{m-1} - \tilde{u}_{n-1}|) \right\} \frac{(t-\xi)^\alpha}{\Gamma(1+\alpha)} \, d\xi.$$

By employing the Integral Mean Value Theorem on the preceding equation, the following outcome is derived.

$$\leq \max_{t\epsilon J} \left[\{\tilde{a}(X) \, \delta(|\tilde{u}_{m-1} - \tilde{u}_{n-1}|) + \tilde{b}(X) \, \sigma(|\tilde{u}_{m-1} - \tilde{u}_{n-1}|)\} \, T \right],$$

$$\leq \max_{t\epsilon J} (|\tilde{u}_{m-1} - \tilde{u}_{n-1}|) \{\tilde{a}(X) \, \delta + \tilde{b}(X) \, \sigma\} \, T,$$

$$\leq \beta \, \|\tilde{u}_{m-1} - \tilde{u}_{n-1}\|,$$

Taking $m = n+1$ then

$$\|\tilde{u}_{n+1} - \tilde{u}_n\| \leq \beta \, \|\tilde{u}_n - \tilde{u}_{n-1}\| \leq \beta^2 \|\tilde{u}_{n-1} - \tilde{u}_{n-2}\| \leq \beta^3 \|\tilde{u}_{n-2} - \tilde{u}_{n-3}\| \leq \cdots \ldots \leq \beta^n \|\tilde{u}_1 - \tilde{u}_0\|.$$

By triangle inequality, we have following results.

$$\|\tilde{u}_m - \tilde{u}_n\| \leq \|\tilde{u}_{n+1} - \tilde{u}_n\| + \|\tilde{u}_{n+2} - \tilde{u}_{n+1}\| + \cdots . + \|\tilde{u}_m - \tilde{u}_{m-1}\| \leq \beta^n \|\tilde{u}_1 - \tilde{u}_0\| + \beta^{n+1} \|\tilde{u}_1 - \tilde{u}_0\|$$

$$+ \cdots . + \beta^{m-1} \|\tilde{u}_1 - \tilde{u}_0\| \leq [\beta^n + \beta^{n+1} + \beta^{n+2} + \cdots + \beta^{m-2} + \beta^{m-1}] \|\tilde{u}_1 - \tilde{u}_0\|,$$

$$\leq \beta^n [1 + \beta + \beta^2 + \cdots + . \beta^{m-n-2} + \beta^{m-n-1}] \|\tilde{u}_1 - \tilde{u}_0\|,$$

$$\leq \beta^n \left[\frac{1 - \beta^{m-n-1}}{1 - \beta} \right] \|\tilde{u}_1 - \tilde{u}_0\|.$$

as $0 < \beta < 1$, so $1 - \beta^{m-n-1} < 1$. Using this we finally obtained

$\|\tilde{u}_m - \tilde{u}_n\| \leq \frac{\beta^n}{1-\beta} \|\tilde{u}_1 - \tilde{u}_0\|$. Since $\|\tilde{u}_1 - \tilde{u}_0\| < \infty$ and so $\|\tilde{u}_m - \tilde{u}_n\| < \infty$ if $m \to \infty$.

Hence the sequence $\{\tilde{u}_n\}$ is a Cauchy sequence in C[J]implying its convergence.

5. Laplace Homotopy Perturbation Method on Fuzzy Time Fractional Advection-Diffusion Equations

This show case the efficacy of our approach by employing the LHPM to construct fuzzy approximate solutions of FTFADE. To achieve this, we utilize the Caputo formula for time fractional derivatives in the application of the Laplace transform (Podlubny, 1998). Continuing with our approach, we employ the Laplace transform on Equation (1) as shown below:

$$L[D_t{}^\alpha \tilde{u}(X,t)] = L\left[\tilde{a}(X) D_X \tilde{u}(X,t) + \tilde{b}(X) D_{XX} \tilde{u}(X,t) + \tilde{q}(X,t)\right] \quad (8)$$

By utilizing Laplace transform properties in the context of the fractional Caputo derivative, the following results are achieved.

$$s^\alpha \tilde{U}(X,s) - s^{\alpha-1} \tilde{u}(X,0) = L\left[\tilde{a}(X) D_x \tilde{u}(X,t) + \tilde{b}(X) D_{XX} \tilde{u}(X,t) + \tilde{q}(X,t)\right] \quad (9)$$

where, $L(\tilde{u}(\mathcal{X},t)) = \tilde{U}(\mathcal{X},s)$ and $L(\tilde{q}(\mathcal{X},t)) = \tilde{Q}(\mathcal{X},s)$.

$$\tilde{U}(\mathcal{X},s) = \frac{\tilde{Q}(\mathcal{X},s)}{s^{\alpha}} + \frac{\tilde{g}(\mathcal{X})}{s} + \frac{1}{s^{\alpha}} L\left[\tilde{a}(\mathcal{X}) D_{\mathcal{X}} \tilde{u}(\mathcal{X},t) + \tilde{b}(\mathcal{X}) D_{\mathcal{X}\mathcal{X}} \tilde{u}(\mathcal{X},t)\right] \quad (10)$$

After applying the Inverse Laplace transform to the previously mentioned equation, we obtain the following result:

$$\tilde{u}(\mathcal{X},t) = L^{-1}\left[\frac{\tilde{Q}(\mathcal{X},s)}{s^{\alpha}} + \frac{\tilde{g}(\mathcal{X})}{s}\right] + L^{-1}\left[\frac{1}{s^{\alpha}} L\left[\tilde{a}(\mathcal{X}) D_{\mathcal{X}} \tilde{u}(\mathcal{X},t) + \tilde{b}(\mathcal{X}) D_{\mathcal{X}\mathcal{X}} \tilde{u}(\mathcal{X},t)\right]\right] \quad (11)$$

The homotopy of Equation (11) is formulated as:

$$H(v,p) = \tilde{u}(\mathcal{X},t) - L^{-1}\left[\frac{\tilde{Q}(\mathcal{X},s)}{s^{\alpha}} + \frac{\tilde{g}(\mathcal{X})}{s}\right] - pL^{-1}\left[\frac{1}{s^{\alpha}} L\left[\tilde{a}(\mathcal{X}) D_{\mathcal{X}} \tilde{u}(\mathcal{X},t) + \tilde{b}(\mathcal{X}) D_{\mathcal{X}\mathcal{X}} \tilde{u}(\mathcal{X},t)\right]\right] = 0 \quad (12)$$

Considering the perturbation method, we adopt the following approach:

$$\tilde{u}(\mathcal{X},t) = \sum_{n=0}^{\infty} p^n \tilde{u}_n(\mathcal{X},t) = p^0 \tilde{u}_0(\mathcal{X},t) + p^1 \tilde{u}_1(\mathcal{X},t) + p^2 \tilde{u}_2(\mathcal{X},t) + \cdots + \cdots \quad (13)$$

After applying the perturbation method to Equation (12) and compiling coefficients of $p^0, p^1, p^2, .. p^n$,these coefficients and other terms are substituted into Equation (13). Subsequently, the embedded parameter *p* approaches 1. The resulting series form represents the approximate solution, also known as the LHPM solution or Fuzzy solution of the FTFADE.

$$\tilde{u}(\mathcal{X},t) = \tilde{u}_0(\mathcal{X},t) + \tilde{u}_1(\mathcal{X},t) + \tilde{u}_2(\mathcal{X},t) + \tilde{u}_3(\mathcal{X},t) + \ldots \quad (14)$$

The series solution incorporating fuzziness and bounded by lower and upper limits is depicted as follows (Salahshour et al., 2012a; Hoa et al., 2019; Vu et al., 2022):

$$\underline{u}(\mathcal{X},t) = \underline{u}_0(\mathcal{X},t) + \underline{u}_1(\mathcal{X},t) + \underline{u}_2(\mathcal{X},t) + \ldots \quad (15)$$

$$\overline{u}(\mathcal{X},t) = \overline{u}_0(\mathcal{X},t) + \overline{u}_1(\mathcal{X},t) + \overline{u}_2(\mathcal{X},t)) + \ldots \quad (16)$$

6. Illustrative Examples

In this section, we provide two examples of FTFADE. We utilize our proposed method to assess the fuzzy approximate results for these instances.

Example 1: (İbiş & Bayram, 2014; and Zureigat et al., 2021): Let's consider linear FFADE with $\tilde{a}(\mathcal{X})$=-1, $\tilde{b}(\mathcal{X}) = 0$ and $\tilde{q}(\mathcal{X},t) = \tilde{k}(r)(sin(\mathcal{X}) + t\,cos(\mathcal{X}))$ in Equation (1):

$$D_t^{\alpha} \tilde{u}(\mathcal{X},t) + \tilde{u}_{\mathcal{X}}(\mathcal{X},t) = \tilde{k}(r)\left[\frac{t^{1-\alpha}}{\Gamma(2-\alpha)} sin(\mathcal{X}) + t\,cos(\mathcal{X})\right], t > 0, \mathcal{X} \in R, 0 < \alpha \leq 1 \quad (17)$$

with boundary conditions: $\tilde{u}(0,t) = \tilde{u}(l,t) = 0$ and fuzzy initial conditions as

$$\tilde{u}(\mathcal{X},0) = \tilde{0}[r-1, 1-r] = \tilde{k}(r) = 0 \quad (18)$$

From (Kirtiwant et al., 2017)

$$\tilde{k}(r) = \tilde{k} = \left[\underline{k}(r), \overline{k}(r)\right], \underline{k}(r) = r - 1, \overline{k}(r) = 1 - r. \quad (19)$$

The exact solution to Equation (18) is stated as:

$$u(\mathcal{X},t) = t\,sin(\mathcal{X}) \quad (20)$$

***Proof*:** To establish the solution, we consider the Laplace transform to apply on Equation (18).

$$L(D_t{}^{\alpha}\tilde{u}(\mathcal{X},t)) + L(\tilde{u}_{\mathcal{X}}(\mathcal{X},t)) = \left[\tilde{k}(r)\left[\frac{t^{1-\alpha}}{\Gamma(2-\alpha)}sin(\mathcal{X}) + t\,cos\mathcal{X}\right]\right] \quad (21)$$

By substituting the initial condition and subsequently performing the inverse Laplace transform, we attain the following result:

$$\tilde{u}(\mathcal{X},t) = L^{-1}\left[\frac{1}{s^{\alpha}}L\left[\tilde{k}(r)\left[\frac{t^{1-\alpha}}{\Gamma(2-\alpha)}sin(\mathcal{X}) + cos(\mathcal{X})\right]\right]\right] - L^{-1}\left[\frac{1}{s^{\alpha}}L\big(D_x(\tilde{u},t)\big)\right] \quad (22)$$

Applying the Homotopy and Perturbation Method, $0 \le p \le 1$, to Equation (22), we arrive at the following result.

$$\sum_{n=0}^{\infty} p^n\,\tilde{u}_n(\mathcal{X},t) = L^{-1}\left[\frac{1}{s^{\alpha}}L\left[\tilde{k}(r)\left[\frac{t^{1-\alpha}}{\Gamma(2-\alpha)}sin(\mathcal{X}) + t\,cos(\mathcal{X})\right]\right]\right] - pL^{-1}\left[\frac{1}{s^{\alpha}}L\big(D_x(\sum_{n=0}^{\infty} p^n\,\tilde{u}_n(\mathcal{X},t))\big)\right] \quad (23)$$

After comparing the coefficients of $p^n, n = 0,1,2,3,4,5$, the results for the coefficient of $p^0$is as follows:

$$\tilde{u}_0(\mathcal{X},t) = \tilde{k}(r)\left[\, t\,sin(\mathcal{X}) + \frac{t^{\alpha+1}}{\Gamma(\alpha+2)}cos(\mathcal{X})\right] \quad (24)$$

Since $\bar{u}_0(\mathcal{X},t:r)$ and $\underline{u}_0(\mathcal{X},t:r)$, upper and lower bounds of $\tilde{u}_0(\mathcal{X},t)$

$$\bar{u}_0(\mathcal{X},t:r) = \bar{k}(r)\left[t\,sin(\mathcal{X}) + \frac{t^{\alpha+1}}{\Gamma(\alpha+2)}cos(\mathcal{X})\right],$$

$$\underline{u}_0(\mathcal{X},t:r) = \underline{k}(r)\left[t\,sin(\mathcal{X}) + \frac{t^{\alpha+1}}{\Gamma(\alpha+2)}cos(\mathcal{X})\right] \quad (25)$$

Further we compare another coefficient of p^1, p^2, p^3, p^4, p^5so on. The approximate fuzzy solution upto 5 steps are obtained as: The coefficient of p^1 yields the upper and lower bounds of $\tilde{u}_1(\mathcal{X},t)$ as follows:

$$\bar{u}_1(\mathcal{X},t:r) = \bar{k}(r)\left[\frac{t^{2\alpha+1}}{\Gamma(2\alpha+2)}sin(\mathcal{X}) - \frac{t^{\alpha+1}}{\Gamma(\alpha+2)}cos(\mathcal{X})\right],$$

$$\underline{u}_1(\mathcal{X},t:r) = \underline{k}(r)\left[\frac{t^{2\alpha+1}}{\Gamma(2\alpha+2)}\sin(\mathcal{X}) - \frac{t^{\alpha+1}}{\Gamma(\alpha+2)}\cos(\mathcal{X})\right] \quad (26)$$

Coefficient of p^2: upper and lower bounds of $\tilde{u}_2(\mathcal{X},t)$ are

$$\bar{u}_2(\mathcal{X},t:r) = \bar{k}(r)\left[-\frac{t^{2\alpha+1}}{\Gamma(2\alpha+2)}\sin(\mathcal{X}) - \frac{t^{3\alpha+1}}{\Gamma(3\alpha+2)}\cos(\mathcal{X})\right],$$

$$\underline{u}_2(\mathcal{X},t:r) = \underline{k}(r)\left[-\frac{t^{2\alpha+1}}{\Gamma(2\alpha+2)}\sin(\mathcal{X}) - \frac{t^{3\alpha+1}}{\Gamma(3\alpha+2)}\cos(\mathcal{X})\right] \quad (27)$$

Coefficient of p^3: upper and lower bounds of $\tilde{u}_3(\mathcal{X},t)$ are.

$$\bar{u}_3(\mathcal{X},t:r) = \bar{k}(r)\left[-\frac{t^{4\alpha+1}}{\Gamma(4\alpha+2)}sin(\mathcal{X}) + \frac{t^{3\alpha+1}}{\Gamma(3\alpha+2)}cos(\mathcal{X})\right],$$

$$\underline{u}_3(\mathcal{X},t:r) = \underline{k}(r)\left[-\frac{t^{4\alpha+1}}{\Gamma(4\alpha+2)}sin(\mathcal{X}) + \frac{t^{3\alpha+1}}{\Gamma(3\alpha+2)}cos(\mathcal{X})\right] \quad (28)$$

Coefficient of p^4: upper and lower bounds of $\tilde{u}_4(\mathcal{X},t)$ are.

$$\bar{u}_4(\mathcal{X},t:r) = \bar{k}(r)\left[\frac{t^{4\alpha+1}}{\Gamma(4\alpha+2)}sin(\mathcal{X}) + \frac{t^{5\alpha+1}}{\Gamma(5\alpha+2)}cos(\mathcal{X})\right],$$

$$\underline{u}_4(\mathcal{X},t;r) = \underline{k}(r)\left[\frac{t^{4\alpha+1}}{\Gamma(4\alpha+2)}sin(\mathcal{X}) + \frac{t^{5\alpha+1}}{\Gamma(5\alpha+2)}cos(\mathcal{X})\right] \tag{29}$$

Coefficient of p^5: upper and lower bounds of $\tilde{u}_5(\mathcal{X},t)$ are.

$$\bar{u}_5(\mathcal{X},t;r) = \bar{k}(r)\left[\frac{t^{6\alpha+1}}{\Gamma(6\alpha+2)}sin(\mathcal{X}) - \frac{t^{5\alpha+1}}{\Gamma(5\alpha+2)}cos(\mathcal{X})\right],$$

$$\underline{u}_5(\mathcal{X},t;r) = \underline{k}(r)\left[\frac{t^{6\alpha+1}}{\Gamma(6\alpha+2)}sin(\mathcal{X}) - \frac{t^{5\alpha+1}}{\Gamma(5\alpha+2)}cos(\mathcal{X})\right] \tag{30}$$

By utilizing these coefficients in both Equations (15) and (16) we derive a fuzzy approximate solution for FTFADE. The resulting solution encompasses both the upper and lower bounds expressed as:

$$\overline{u}(\mathcal{X},t;r) = \overline{k}(r)\left[t\,sin(\mathcal{X}) + \frac{t^{6\alpha+1}}{\Gamma(6\alpha+2)}sin(\mathcal{X}) + \ldots\right] \tag{31}$$

$$\underline{u}(\mathcal{X},t;r) = \underline{k}(r)\left[t\,sin(\mathcal{X}) + \frac{t^{6\alpha+1}}{\Gamma(6\alpha+2)}sin(\mathcal{X}) + ..\right] \tag{32}$$

Subsequently, we will proceed to evaluate the numerical value of the approximate solution for FTFADE, limiting our consideration to the first five terms. This assessment is aimed at gaining a clear understanding of the effectiveness of LHPM in addressing FFPDE. To enhance comprehension, we provide graphical representations of $\overline{u}(\mathcal{X},t;r)$ and $\underline{u}(\mathcal{X},t;r)$ in **Figures 1** and **2** while varying the values of α (0.6, 0.8, 0.9, 0.95, and 1) across different levels of uncertainty r.

Example 2: Consider one dimensional linear fuzzy fractional ADE (İbiş & Bayram, 2014) and (Zureigat et al., 2021):

$$D_t{}^{\alpha}\tilde{u}(\mathcal{X},t) = -\tilde{u}_{\mathcal{X}}(\mathcal{X},t) + \tilde{u}_{\mathcal{X}\mathcal{X}}(\mathcal{X},t)\,, t > 0, \mathcal{X} \in R \tag{33}$$

with $0 < \alpha \leq 1$ and fuzzy initial conditions:

$$\tilde{u}(\mathcal{X},0) = \tilde{k}(r)e^{-\mathcal{X}} \tag{34}$$

and

$$\tilde{k}(r) = \left[\underline{k}(r), \overline{k}(r)\right] \tag{35}$$

The exact solution of Equation (33) (Singh, 2022) is

$$\tilde{u}(\mathcal{X},t) = e^{-\mathcal{X}}e^{2t} \tag{36}$$

The computed upper and lower bounds of fuzzy approximate solution of this case are as:

$$\bar{\boldsymbol{u}}(\boldsymbol{\mathcal{X}},\boldsymbol{t};\boldsymbol{r}) = \bar{\boldsymbol{k}}(\boldsymbol{r})\boldsymbol{e}^{-\boldsymbol{\mathcal{X}}}\left[\begin{matrix}\mathbf{1} + \frac{\mathbf{2}\boldsymbol{t}^{\boldsymbol{\alpha}}}{\boldsymbol{\Gamma}(\boldsymbol{\alpha}+\mathbf{1})} + \frac{\mathbf{4}\boldsymbol{t}^{\mathbf{2}\boldsymbol{\alpha}}}{\boldsymbol{\Gamma}(\mathbf{2}\boldsymbol{\alpha}+\mathbf{1})} + \frac{\mathbf{8}\boldsymbol{t}^{\mathbf{3}\boldsymbol{\alpha}}}{\boldsymbol{\Gamma}(\mathbf{3}\boldsymbol{\alpha}+\mathbf{1})} \\ + \frac{\mathbf{16}\boldsymbol{t}^{\mathbf{4}\boldsymbol{\alpha}}}{\boldsymbol{\Gamma}(\mathbf{4}\boldsymbol{\alpha}+\mathbf{1})} + \frac{\mathbf{32}\boldsymbol{t}^{\mathbf{5}\boldsymbol{\alpha}}}{\boldsymbol{\Gamma}(\mathbf{5}\boldsymbol{\alpha}+\mathbf{1})} + \ldots\ldots\ldots\end{matrix}\right] \tag{37}$$

$$\underline{u}(\mathcal{X},t;r) = \underline{k}(r)e^{-\mathcal{X}}\left[\begin{matrix}1 + \frac{2t^{\alpha}}{\Gamma(\alpha+1)} + \frac{4t^{2\alpha}}{\Gamma(2\alpha+1)} + \frac{8t^{3\alpha}}{\Gamma(3\alpha+1)} \\ + \frac{16t^{4\alpha}}{\Gamma(4\alpha+1)} + \frac{32t^{5\alpha}}{\Gamma(5\alpha+1)} + \ldots\ldots\ldots\end{matrix}\right] \tag{38}$$

The fuzzy approximate solution of FTFADE coincides exactly with the results obtained from Fractional ADE as discussed by (İbiş & Bayram, 2014).In the next section we provide graphical representations of $\overline{u}(\mathcal{X},t;r)$ and $\underline{u}(\mathcal{X},t;r)$ varying at the values of α (0.6, 0.8, 0.9, 0.95, and 1) across different levels of uncertainty r in **Figures 3** and **4**.

7. Result Analysis

In this section, we conduct a numerical analysis for the LHPM solution to the FTFADE cases discussed in the previous section. The numerical values and surface graphs are obtained using MATHEMATICA 11.3 and Microsoft Excel. To facilitate comparison, **Table 3** presents the exact solutions for the two cases of FTFADE, while **Tables 1** and **2** display lower, upper bounds of the fuzzy LHPM solutions. Furthermore, to validate our proposed analysis, 3D surface graphs of the approximate solution are generated at different fractional orders for both cases, considering different levels of uncertainty and time while holding $\mathcal{X}$constant. **Figures 1-10** depict the numerical approximations to the solutions of the cases. Specifically, **Figures 1-2** illustrate the LHPM solutions for example 1, while **Figures 3-4** showcase the LHPM solutions for example 2. The variations in time (t) and r- level (uncertainty) range from 0 to 1, corresponding to various fractional orders considered in the analysis. Using these figures, we can visually comprehend the influence of uncertainty at various fractional orders. The upper surface and lower surface plots situated above and below the cusp value (r = 1), portray the solutions as $\overline{u}(\mathcal{X}, t; r)$ and $\underline{u}(\mathcal{X}, t; r)$ respectively. It is intriguing to note the striking similarities in the fuzzy solutions depicted in the surface graphs above and below the cusp at r = 1, as shown in **Figures 1-2** and **3-4** for both cases at different fractional orders. These surface graphs serve as compelling evidence of the accuracy and efficiency of the LHPM.

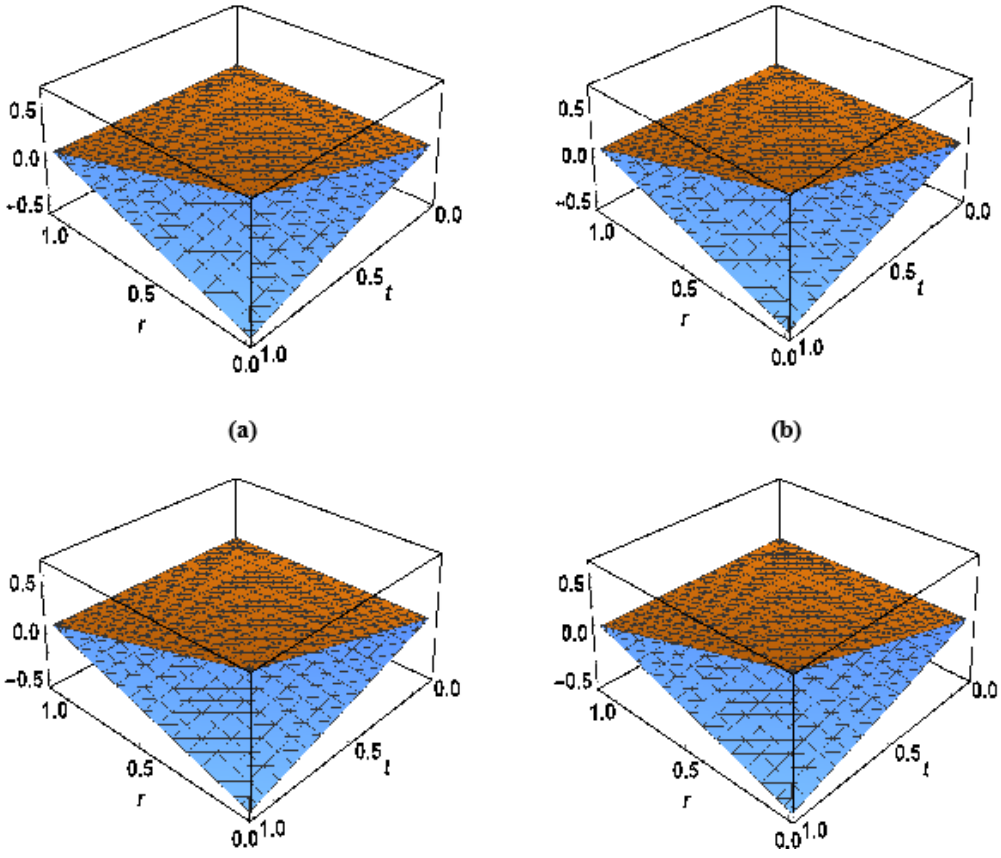

Figure 1. Fuzzy LHPM solution, $\bar{u}(\mathcal{X}, t: r)$ and $\underline{u}(\mathcal{X}, t: r)$ of Example 1 at a) α = 0.6, b) α = 0.8, c) α = 0.9 and d) α= 0.95 keeping $\mathcal{X} = 0.7$.

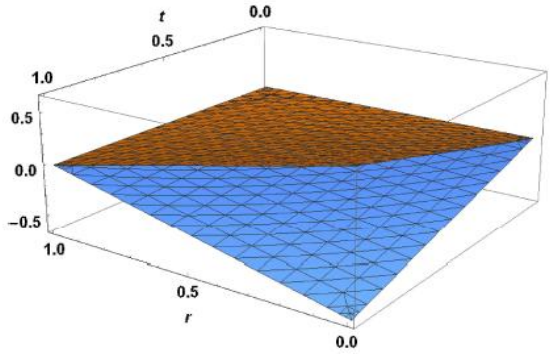

Figure 2. Fuzzy LHPM solution, $\bar{u}(\mathcal{X}, t: \mathcal{r})$ and $\underline{u}(\mathcal{X}, t: \mathcal{r})$ of Example 1, $\alpha = 1$, with $\mathcal{X} = 0.7$.

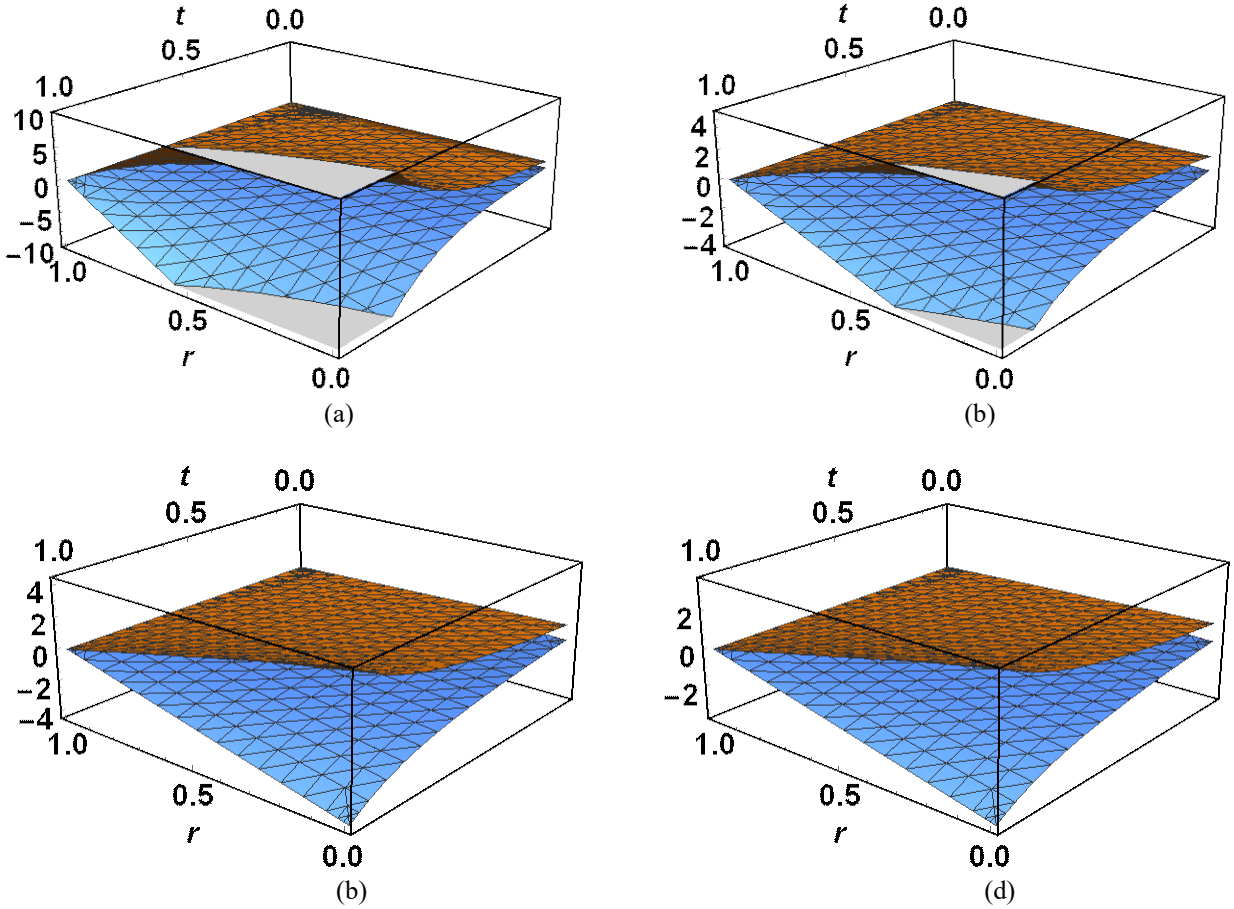

Figure 3. Fuzzy LHPM solution, $\bar{u}(\mathcal{X}, t: \mathcal{r})$ and $\underline{u}(\mathcal{X}, t: \mathcal{r})$of Example 2 at (a) $\alpha = 0.6$, (b) $\alpha = 0.8$, (c) $\alpha = 0.9$ and (d) $\alpha = 0.95$, keeping $\mathcal{X} = 0.7$.

Numerical value of $\bar{u}(x, t: \mathcal{r})$, representing the upper bound of the fuzzy solution in FTFADE, is used for comparison with the exact solution of ADE.

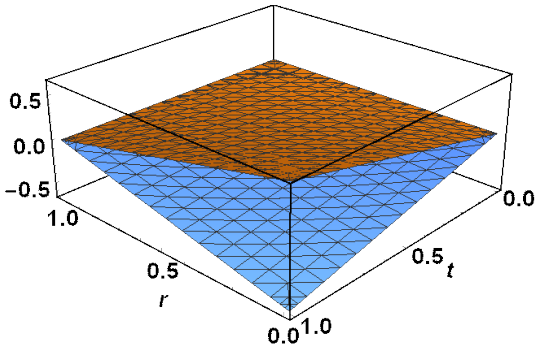

Figure 4. Fuzzy LHPM solution, $\bar{u}(\mathcal{X}, t; \mathcal{r})$ and $\underline{u}(\mathcal{X}, t; \mathcal{r})$ of Example 2, $\alpha = 1$, with $\mathcal{X} = 0.7$.

Notably, when $\mathcal{r} = 0$ and $\alpha = 1$, **Figure 5** exhibits a striking resemblance to **Figure 6**, which displays the exact solution of Example 1. This remarkable similarity is evident, even though we only computed the estimated solution up to the first five terms.

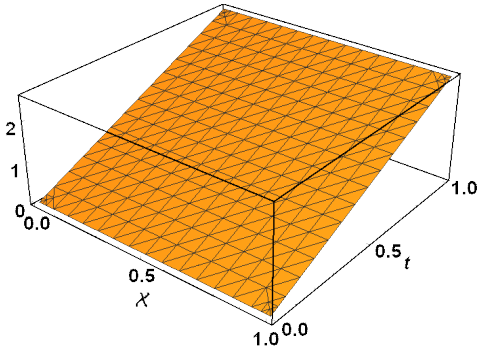

Figure 5. Fuzzy approximation upper bound of example 1.

Furthermore, upon observing **Figures 7** and **8**, it becomes evident that the pattern in upper bound solution with $\mathcal{r} = 0$ and $\alpha = 1$closely resembles the exact solution for example 2. These graphical findings serve as strong indicators that the LHPM is a highly reliable and robust approach for solving FTFADE. We observed that in both cases, the numerical results obtained from proposed method align perfectly with those derived from the ADE solution when $\mathcal{r} = 0$, further affirming the accuracy and effectiveness of the LHPM method in handling such scenarios.

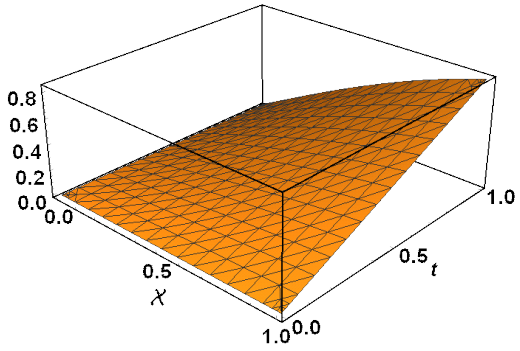

Figure 6. Fuzzy approximation exact outcome of example 1.

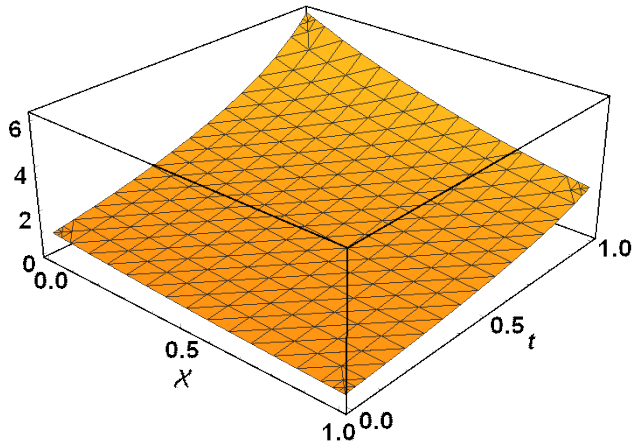

Figure 7. Fuzzy approximation upper bound of example 2.

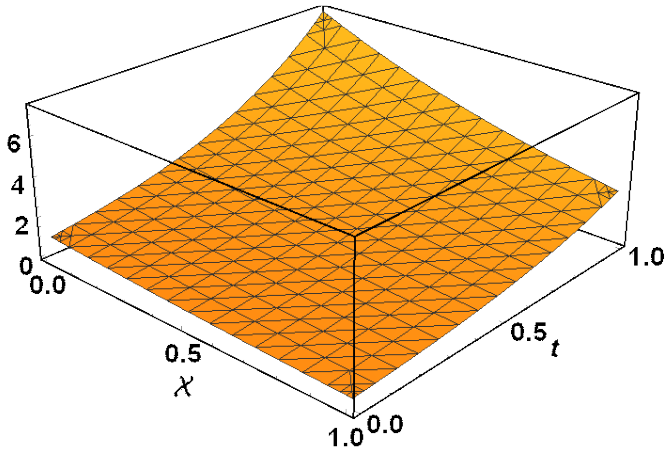

Figure 8. Exact outcome of example 2.

In the illustrative cases, to perform numerical computations, the infinite power series in Equations (31) to (32) and Equations (37) to (38) were truncated up to finite terms. In case 1, **Table 1** shows both bounds of fuzzy numerical results, while **Table 2** provides the corresponding bounds for case 2. The computed fuzzy numerical results are shown for different r -levels ranging from 0 to 1.In particular, the analysis focuses on the Fuzzy LHPM solutions for various fractional orders in Example 1, **Table 1** contains the values for the upper and lower fuzzy LHPM solutions, denoted as $\overline{u}(X,t:r)$ and $\underline{u}(X,t:r)$ respectively, at different r- levels while keeping$X$ = 0.7 and t = 0.5. Notably, the absolute numerical values of $\overline{u}(X,t:r)$ and $\underline{u}(X,t:r)$are precisely the same. For example, at fractional order α = 0.8 and r = 0.4, the numerical value of $\overline{u}(X,t:r)$ and$\underline{u}(X,t:r)$ are 0.1948243 and -0.1948243, respectively, which are numerically equal. Additionally, **Table 1** presents the approximate upper bound solution for r = 0.6 at various fractional orders α (0.6, 0.8, 0.9, 0.95, and 1) as 0.13294, 0.1298829, 0.1293999, 0.1292549, and 0.1291495, respectively. These approximate upper bounds decrease significantly as the fractional order increases. Furthermore, it is observed that the approximate lower bound solution for r = 0.6 at various fractional orders also decreases substantially.

Table 1. The lower bound and upper bound of fuzzy numerical solution of example 1, keeping $\mathcal{X} = 0.7$ and $t = 0.5$.

$U(\mathcal{X}, t; r)$										
$\alpha \rightarrow$	0.6		0.8		0.9		0.95		1	
r-level ↓	$\underline{u}(\mathcal{X}, t; r)$	$\overline{u}(\mathcal{X}, t; r)$	$\underline{u}(\mathcal{X}, t; r)$	$\overline{u}(\mathcal{X}, t; r)$	$\underline{u}(\mathcal{X}, t; r)$	$\overline{u}(\mathcal{X}, t; r)$	$\underline{u}(\mathcal{X}, t; r)$	$\overline{u}(\mathcal{X}, t; r)$	$\underline{u}(\mathcal{X}, t; r)$	$\overline{u}(\mathcal{X}, t; r)$
0	-0.33235	0.33235	-0.3247072	0.3247072	-0.3234999	0.3234999	-0.3231374	0.3231374	-0.3228738	0.3228738
0.1	-0.299115	0.299115	-0.2922365	0.2922365	-0.2911499	0.2911499	-0.2908236	0.2908236	-0.2905864	0.2905864
0.2	-0.26588	0.26588	-0.2597658	0.2597658	-0.2587999	0.2587999	-0.2585099	0.2585099	-0.2582991	0.2582991
0.3	-0.232645	0.232645	-0.2272951	0.2272951	-0.2264499	0.2264499	-0.2261962	0.2261962	-0.2260117	0.2260117
0.4	-0.19941	0.19941	-0.1948243	0.1948243	-0.1940999	0.1940999	-0.1938824	0.1938824	-0.1937243	0.1937243
0.5	-0.166175	0.166175	-0.1623536	0.1623536	-0.1617499	0.1617499	-0.1615687	0.1615687	-0.1614369	0.1614369
0.6	-0.13294	0.13294	-0.1298829	0.1298829	-0.1293999	0.1293999	-0.1292549	0.1292549	-0.1291495	0.1291495
0.7	-0.099705	0.099705	-0.0974122	0.0974122	-0.09705	0.09705	-0.0969412	0.0969412	-0.0968621	0.0968621
0.8	-0.06647	0.06647	-0.0649414	0.0649414	-0.0647	0.0647	-0.0646275	0.0646275	-0.0645748	0.0645748
0.9	-0.033235	0.033235	-0.0324707	0.0324707	-0.03235	0.03235	-0.0323137	0.0323137	-0.0322874	0.0322874
1	0	0	0	0	0	0	0	0	0	0

Now in **Table 2**, the approximate upper bound solutions for $r = 0.4$ at various fractional orders α(0.6, 0.8, 0.9, 0.95, and 1) are 1.8226, 0.999256, 0.850856, 0.796264, and 0.74943, respectively. Interestingly, the approximate upper bounds decrease substantially as the fractional order increases. Likewise, the approximate lower bound solutions for $r = 0.4$ at various fractional orders also decrease very rapidly.

Table 2. The lower bound and upper bound of fuzzy numerical solution of Example 2, keeping $\mathcal{X} = 0.7$ and $t = 0.5$.

$u(\mathcal{X}, t; r)$										
$\alpha \rightarrow$	0.6		0.8		0.9		0.95		1	
r-level ↓	$\underline{u}(\mathcal{X}, t; r)$	$\overline{u}(\mathcal{X}, t; r)$	$\underline{u}(\mathcal{X}, t; r)$	$\overline{u}(\mathcal{X}, t; r)$	$\underline{u}(\mathcal{X}, t; r)$	$\overline{u}(\mathcal{X}, t; r)$	$\underline{u}(\mathcal{X}, t; r)$	$\overline{u}(\mathcal{X}, t; r)$	$\underline{u}(\mathcal{X}, t; r)$	$\overline{u}(\mathcal{X}, t; r)$
0	-3.03766	3.03766	-1.66543	1.66543	-1.41809	1.41809	-1.32711	1.32711	-1.24905	1.24905
0.1	-2.7339	2.7339	-1.49888	1.49888	-1.27628	1.27628	-1.1944	1.1944	-1.12414	1.12414
0.2	-2.43013	2.43013	-1.33234	1.33234	-1.13447	1.13447	-1.06168	1.06168	-0.99924	0.99924
0.3	-2.12636	2.12636	-1.1658	1.1658	-0.992665	0.992665	-0.928974	0.928974	-0.874335	0.874335
0.4	-1.8226	1.8226	-0.999256	0.999256	-0.850856	0.850856	-0.796264	0.796264	-0.74943	0.74943
0.5	-1.51883	1.51883	-0.832713	0.832713	-0.709046	0.709046	-0.663553	0.663553	-0.624525	0.624525
0.6	-1.33657	1.33657	-0.732787	0.732787	-0.623961	0.623961	-0.583927	0.583927	-0.549582	0.549582
0.7	-0.911299	0.911299	-0.499628	0.499628	-0.425428	0.425428	-0.398132	0.398132	-0.374715	0.374715
0.8	-0.607533	0.607533	-0.333085	0.333085	-0.283619	0.283619	-0.265421	0.265421	-0.24981	0.24981
0.9	-0.303766	0.303766	-0.166543	0.166543	-0.141809	0.141809	-0.132711	0.132711	-0.124905	0.124905
1	0	0	0	0	0	0	0	0	0	0

In both cases, the upper and lower numerical values of LHPM solutions of FTFADE decrease as the fractional order α approaches 1 at a specific r -level. This observation leads us to conclude that the LHPM is a very fast converging method, with its solutions exhibiting remarkable convergence characteristics as the fractional order increases.

Table 3. The precise solutions for the given examples at $\mathcal{X} = 0.7$.

Time	Exact solution		Time	Exact solution	
	Example 1	Example 2		Example 1	Example 1
0	0	0.4965853	0.6	0.386531	1.64872127
0.1	0.064422	0.60653066	0.7	0.450952	2.01375271
0.2	0.128844	0.74081822	0.8	0.515374	2.45960311
0.3	0.193265	0.90483742	0.9	0.579796	3.00416602
0.4	0.257687	1.10517092	1	0.644218	3.66929667
0.5	0.322109	1.34985881			

The Fuzzy LHPM solution of $\overline{u}(\mathcal{X},t:r)$ and $\underline{u}(\mathcal{X},t:r)$ at various fractional orders of both the cases are shown in **Figures 9** and **10** at specific $\mathcal{X}$ and t. The effect of the uncertainty has been shown along with variation in fractional order of the cases through figures. Firstly, in **Figure 9** for example 1, we notice that when the fractional order increases, the graphs of both bounds begin to converge fast as r approaches to cusp. Secondly, as the fractional order is raised, both bounds of the approximate solution move closer to the origin. Finally, as the uncertainty r approaches 1, the solution graph at α = 0.4, 0.6, 0.8, 0.9, 0.95, 1 coincides. However, we observe a similar analysis in **Figure 10** for example 2. It is interesting to conclude that increasing the fractional order, both branches of fuzzy solution converging toward the cusp where r = 1.

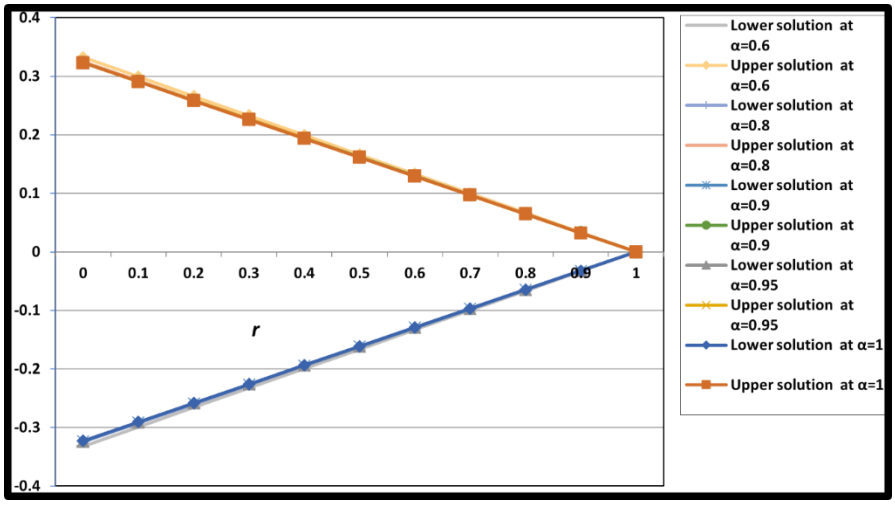

Figure 9. Fuzzy LHPM solutions at α = 0.6 ,0.8, 0.9, 0.95 and 1 at $\mathcal{X}$ = 0.7, t = 0.5 at different r- levels for example 1.

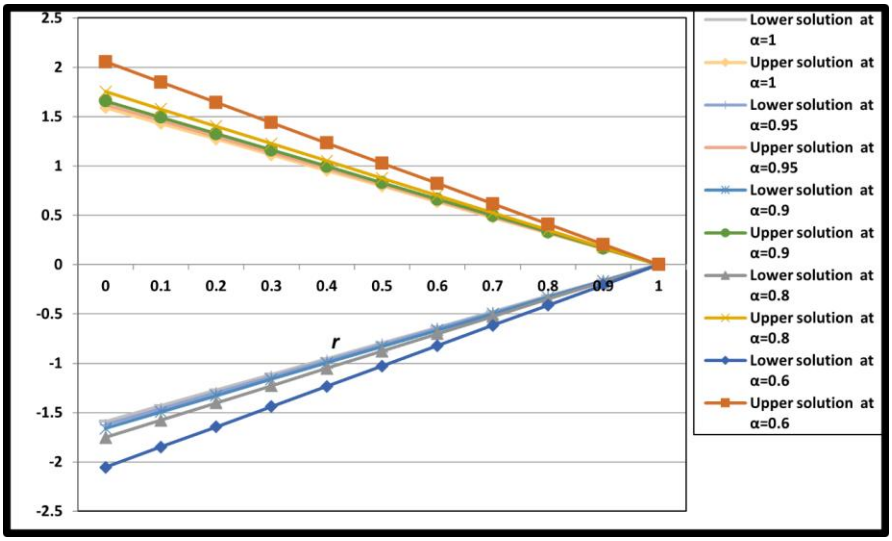

Figure 10. Fuzzy LHPM solutions at α = 0.6, 0.8, 0.9, 0.95 and 1 at $\mathcal{X}$ = 0.7, t = 0.5 at different r- levels for example 2.

The absolute error of the numerical solution is defined as

$$\left[\widetilde{\mathrm{E}}\right]_{r} = |\text{Fuzzy LHPM solution} - \text{Exact solution}|$$

$$\left[\widetilde{\mathrm{E}}\right]_{r} = \begin{cases} [\overline{\mathrm{E}}]_{r} = \left|\overline{u}(\mathcal{X}, t: r) - \overline{k}(r)\text{Exact solution}\right| \\ \left[\underline{\mathrm{E}}\right]_{r} = \left|\underline{u}(\mathcal{X}, t: r) - \underline{k}(r)\text{Exact solution}\right| \end{cases}$$

Table 4. Absolute relative error of lower bound of fuzzy numerical solution with $\underline{k}(r)$ exact solution of example 1, keeping $\mathcal{X}$ = 0.7 and t= 0.5.

$\alpha\rightarrow$	$[\underline{\mathrm{E}}]_{r}$				
	0.6	**0.8**	**0.9**	**0.95**	**1**
r**-level**					
0	0.0102412	0.0025984	0.001391	0.0010285	0.000765
0.1	0.009217	0.0023386	0.0012519	0.0009257	0.0006885
0.2	0.0081929	0.0020787	0.0011128	0.0008228	0.000612
0.3	0.0071688	0.0018189	0.0009737	0.00072	0.0005355
0.4	0.0061447	0.001559	0.0008346	0.0006171	0.000459
0.5	0.0051206	0.0012992	0.0006955	0.0005143	0.0003825
0.6	0.0040965	0.0010394	0.0005564	0.0004114	0.000306
0.7	0.0030723	0.0007795	0.0004173	0.0003086	0.0002295
0.8	0.0020482	0.0005197	0.0002782	0.0002057	0.000153
0.9	0.0010241	0.0002598	0.0001391	0.0001029	7.65E-05
1	0	0	0	0	0

In case 1, in **Table 4**, at distinct fractional order α, absolute errors of lower bound are inclusively analysed, taking $\mathcal{X}$ = 0.7 and t = 0.5 as constant, with$\underline{k}(r)$ Exact solution. At different levels from 0 to 1 the absolute error at fractional order from 0.6 to 1 decrease significantly.

In **Table 5**, absolute relative error of upper bound with exact solution is analysed at distinct fractional order α, with consideration $\mathcal{X}$ = 0.7 and t = 0.5 as constant. At different levels from 0 to 1 the absolute error decrease significantly.

Table 5. Absolute relative error upper bound of fuzzy numerical solution of example 1, keeping $\mathcal{X}$ = 0.7 and t = 0.5.

α	$[\overline{\mathrm{E}}]_{r}$				
	0.6	**0.8**	**0.9**	**0.95**	**1**
r**-level**					
0	0.01024115	0.00259839	0.00139102	0.00102853	0.000764973
0.1	0.00921703	0.00233855	0.00125192	0.00092567	0.000688476
0.2	0.00819292	0.00207871	0.00111282	0.00082282	0.000611979
0.3	0.0071688	0.00181887	0.00097372	0.00071997	0.000535481
0.4	0.00614469	0.00155903	0.00083461	0.00061712	0.000458984
0.5	0.00512057	0.0012992	0.00069551	0.00051426	0.000382487
0.6	0.00409646	0.00103936	0.00055641	0.00041141	0.000305989
0.7	0.00307234	0.00077952	0.00041731	0.00030856	0.000229492
0.8	0.00204823	0.00051968	0.0002782	0.00020571	0.000152995
0.9	0.00102411	0.00025984	0.0001391	0.00010285	0.0000765
1	0	0	0	0	0

In case 2, in **Table 6**, at distinct fractional order α, absolute relative error of lower bound and upper bound with with $\underline{k}(r)$exact solutionis analysed, with $\mathcal{X}$ = 0.7 and t = 0.5. At different levels from 0 to 1 the absolute error at fractional order from 0.6 to 1 decrease significantly. From this Table we can very surely conclude LHPM solution as fast and robust method.

Table 6. Absolute relative error fuzzy numerical solution of example 2, keeping $\mathcal{X}$ = 0.7 and t = 0.5 at different r-level.

α	r-level	$\underline{u}(0.7, 0.5: r)$	$[\underline{E}]_r$	$\overline{u}(0.7, 0.5: r)$	$[\bar{E}]_r$
0.6	0.2	-11.28763517	10.20774812	11.28763517	10.20774812
	0.4	-8.465726377	7.655811093	8.465726377	7.655811093
	0.6	-5.643817585	5.103874062	5.643817585	5.643817585
	0.8	-2.821908792	2.551937031	2.821908792	2.551937031
	1	0	0	0	0
0.8	0.2	-3.002821841	1.922934795	3.002821841	1.922934795
	0.4	-2.252116381	1.442201096	2.252116381	1.442201096
	0.6	-1.501410921	0.961467398	1.501410921	0.961467398
	0.8	-0.75070546	0.480733699	0.75070546	0.480733699
	1	0	0	0	0
0.9	0.2	-1.966978677	0.887091631	1.966978677	0.887091631
	0.4	-1.475234008	0.665318723	1.475234008	0.665318723
	0.6	-0.983489339	0.443545816	0.983489339	0.443545816
	0.8	-0.491744669	0.221772908	0.491744669	0.221772908
	1	0	0	0	0
0.95	0.2	-1.644464746	0.5645777	1.644464746	0.5645777
	0.4	-1.233348559	0.423433275	1.233348559	0.423433275
	0.6	-0.822232373	0.28228885	0.822232373	0.28228885
	0.8	-0.411116186	0.141144425	0.411116186	0.141144425
	1	0	0	0	0
1	0.2	-1.400108873	0.320221827	1.400108873	0.320221827
	0.4	-1.050081655	0.24016637	1.050081655	0.24016637
	0.6	-0.700054437	0.160110914	0.700054437	0.160110914
	0.8	-0.350027218	0.080055457	0.350027218	0.080055457
	1	0	0	0	0

7.1 Numerical Comparison and Validation

To facilitate comparison, **Table 3** presents the exact solutions for the two cases of FTFADE, while **Tables 1** and **2** display lower, upper bounds of the fuzzy LHPM solutions. Furthermore, to validate our proposed analysis, 3D surface graphs of the approximate solution are generated at different fractional orders for both cases, considering different levels of uncertainty and time while holding $\mathcal{X}$ constant. **Figures 1** to **10** depict the numerical approximations to the solutions of the cases. Specifically, **Figures 1** to **2** illustrate the LHPM solutions for example 1, while **Figures 3** to **4** showcase the LHPM solutions for example 2. The variations in time (t) and r- level (uncertainty) range from 0 to 1, corresponding to various fractional orders considered in the analysis. Using these figures, we can visually comprehend the influence of uncertainty at various fractional orders. The upper surface and lower surface plots situated above and below the cusp value (r = 1), portray the solutions as $\bar{u}(\mathcal{X}, t: r)$ and $\underline{u}(\mathcal{X}, t: r)$ respectively.

7.2 Sensitivity Analysis of Fuzzy Parameters

To enhance the practical utility of the proposed model, this section addresses the impact of fuzzy parameters, specifically the average velocity $\tilde{a}(\mathcal{X})$) and the diffusion coefficient $\tilde{b}(\mathcal{X})$, on the solution's behavior. A sensitivity analysis as shown in **Figure 11** is crucial for understanding how uncertainty in these key physical parameters propagates through the model and affects the final fuzzy concentration $\tilde{u}(\mathcal{X}, t)$. Such an analysis would involve systematically varying the uncertainty in $\tilde{a}(\mathcal{X})$and $\tilde{b}(\mathcal{X})$ and observing the corresponding changes in the solution's upper and lower bounds. For instance, one could modify example 1 by defining $\tilde{a}(\mathcal{X})$and $\tilde{b}(\mathcal{X})$ as triangular fuzzy numbers instead of crisp values. The expected outcome is that as the fuzziness (i.e., the spread of the fuzzy number) of the parameters

increases, the spread of the resulting fuzzy solution $\tilde{u}(\mathcal{X}, t)$ will also widen. This demonstrates the model's response to input uncertainty, a vital aspect for real-world applications like contaminant transport, where these coefficients are often imprecisely known.

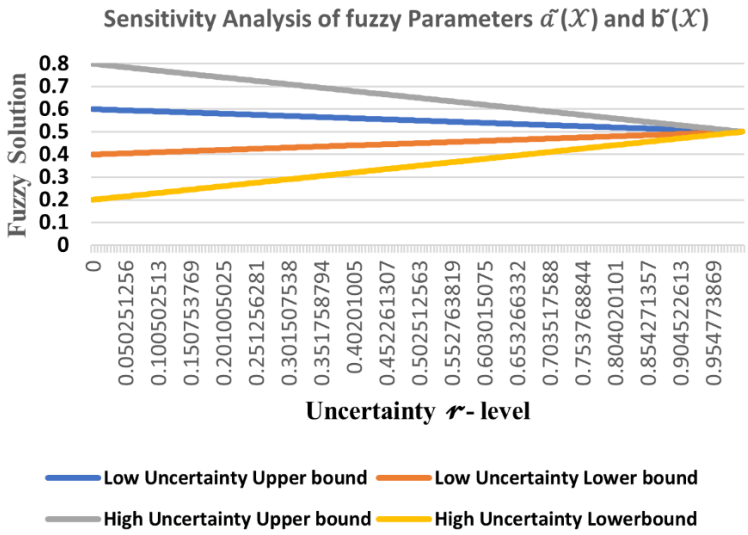

Figure 11. Fuzzy solution $u(\mathcal{X}, t: r)$versus the r-level.

7.3 Comparative Analysis with Existing Methods

To substantiate the claim of novelty and efficiency for the proposed LHPM, **Figure 12** provides a direct quantitative comparison of the Laplace Homotopy Perturbation Method (LHPM) and the Adomian Decomposition Method (ADM) against an exact solution at four distinct uncertainty levels (r -levels).

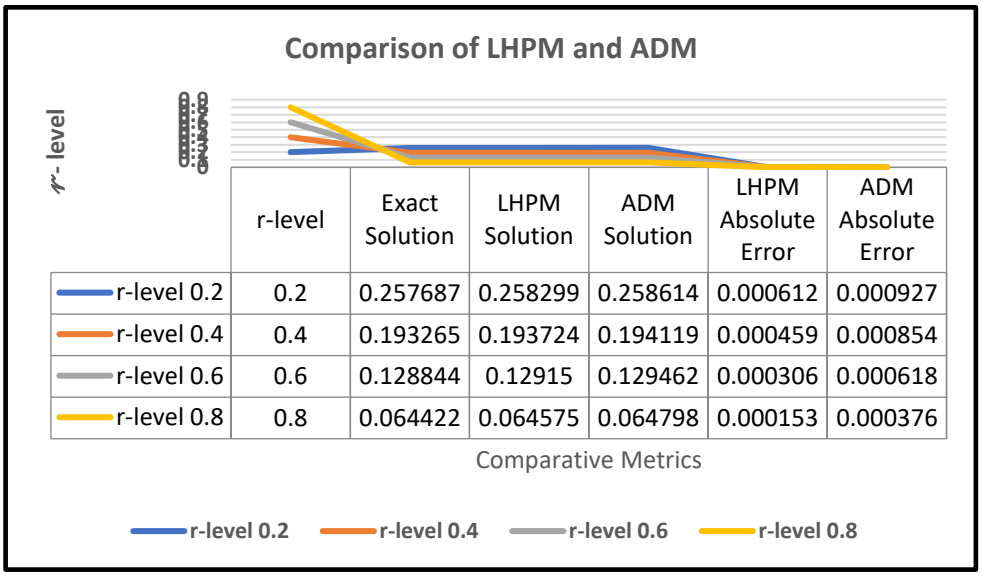

r-level	Exact Solution	LHPM Solution	ADM Solution	LHPM Absolute Error	ADM Absolute Error
r-level 0.2	0.2	0.257687	0.258299	0.258614	0.000612	0.000927
r-level 0.4	0.4	0.193265	0.193724	0.194119	0.000459	0.000854
r-level 0.6	0.6	0.128844	0.12915	0.129462	0.000306	0.000618
r-level 0.8	0.8	0.064422	0.064575	0.064798	0.000153	0.000376

Figure 12. Comparison of LHPM and ADM solutions and their absolute errors for example 1 at various r-levels with constant $\alpha = 1$, $\mathcal{X} = 0.7$, $t = 0.5$.

Figure 12 provides a direct quantitative comparison of the Laplace Homotopy Perturbation Method (LHPM) and the Adomian Decomposition Method (ADM) against an exact solution at four distinct uncertainty levels (r -levels). The primary and most significant conclusion are the superior accuracy of the LHPM. For every r -level 0.2, 0.4, 0.6, and 0.8 the absolute error associated with the LHPM solution is consistently lower than that of the ADM. For example, at an r -level of 0.4, the LHPM error is 0.000459, which is substantially smaller than the ADM error of 0.000854. This demonstrates that the LHPM yields a more accurate result and deviates less from the exact solution compared to the ADM.

8. Limitations and Future Research Directions

The analysis is confined to one-dimensional, linear Fuzzy Time-Fractional Advection-Diffusion Equations (FTFADEs). Future work should extend the LHPM to multi-dimensional and nonlinear systems, which are more representative of real-world phenomena. Additionally, the advection and diffusion coefficients in the illustrative examples were treated as crisp, non-fuzzy values. A more robust validation would implement these parameters as fuzzy numbers to fully model system uncertainty.

Finally, the comparative analysis was limited, benchmarking the LHPM solely against the Adomian Decomposition Method (ADM). Future studies could provide a more comprehensive performance profile by including comparisons with other techniques like the Variational Iteration Method (VIM). Addressing these aspects will broaden the method's applicability and further validate its effectiveness.

9. Conclusion

In the present research article, we provide a novel method to analyse the approximate and numerical solution of FTFADE using Caputo fractional derivative. Additionally, we have obtained sufficient condition for the uniqueness of the solution. Moreover, by leveraging the fixed-point theorem, we have demonstrated the convergence of the proposed method. This approach exhibits both efficiency and accuracy, manifesting a remarkable correspondence between the numerical approximations and exact solutions across different fractional orders. To further support our findings, we have illustrated our results with examples involving FTFADE. The outcomes of the examples numerically and graphically justify the pertinence, precision, robustness, and effectiveness of our approach. Notably, this approach has broader applicability, thus, can be extended to other fuzzy linear and nonlinear fractional order equations. This extension promises to yield informative results across various fields, including financial modelling. The proposed method presents researchers with a valuable tool to obtain efficient and accurate solutions for complex equations involving uncertain parameters, contributing to advancements in research and problem-solving in relevant field.

Conflicts of Interest

The authors declare that they have no known competing financial interests or personal relationships that could have appeared to influence the work reported in this paper.

Acknowledgements

The author Dr Nahid Fatima would like to thank Prine sultan university for paying APC through TAS lab.

AI Disclosure

The author(s) declare that no assistance is taken from generative AI to write this article.

References

Aghdam, Y.E., Mesgrani, H., Javidi, M., & Nikan, O. (2021). A computational approach for the space-time fractional advection–diffusion equation arising in contaminant transport through porous media. *Engineering with Computers*, *37*(4), 3615-3627. https://doi.org/10.1007/s00366-020-01021-y.

Ahmad, I., Ali, Z., Khan, B., Shah, K., & Abdeljawad, T. (2025). Exploring the dynamics of Gumboro-Salmonella co-infection with fractal fractional analysis. *Alexandria Engineering Journal*, *117*, 472-489. https://doi.org/10.1016/j.aej.2024.12.119.

Ahmad, S., Ullah, A., Ullah, A., Akgül, A., & Abdeljawad, T. (2021). Computational analysis of fuzzy fractional order non-dimensional Fisher equation. *Physica Scripta*, *96*(8), 084004. https://doi.org/10.1088/1402-4896/abface.

Ahmadian, A., Salahshour, S., Chan, C.S., & Baleanu, D. (2018). Numerical solutions of fuzzy differential equations by an efficient Runge–Kutta method with generalized differentiability. *Fuzzy Sets and Systems*, *331*, 47-67. https://doi.org/10.1016/j.fss.2016.11.013.

Alikhani, R., & Bahrami, F. (2013). Global solutions for nonlinear fuzzy fractional integral and integrodifferential equations. *Communications in Nonlinear* Science *and Numerical Simulation*, *18*(8), 2007-2017. https://doi.org/10.1016/j.cnsns.2012.12.026.

Allahviranloo, T., & Ghanbari, B. (2020). On the fuzzy fractional differential equation with interval Atangana–Baleanu fractional derivative approach. *Chaos, Solitons & Fractals*, *130*, 109397. https://doi.org/10.1016/j.chaos.2019.109397.

Arfan, M., Shah, K., Abdeljawad, T., & Hammouch, Z. (2021). An efficient tool for solving two-dimensional fuzzy fractional-ordered heat equation. *Numerical Methods for Partial Differential Equations*, *37*(2), 1407-1418.

Babolian, E., Sadeghi, H., & Javadi, S. (2004). Numerically solution of fuzzy differential equations by Adomian method. *Applied Mathematics and Computation*, *149*(2), 547-557. https://doi.org/10.1016/S0096-3003(03)00160-7.

Bilal, M., Iqbal, J., Shah, K., Abdalla, B., Abdeljawad, T., & Ullah, I. (2024). Analytical solutions of the space–time fractional Kundu–Eckhaus equation by using modified extended direct algebraic method. *Partial Differential Equations in Applied Mathematics*, *11*, 100832. https://doi.org/10.1016/j.padiff.2024.100832.

Chakraverty, S., Tapaswini, S., & Behera, D. (2016). *Fuzzy arbitrary order system: fuzzy fractional differential equations and applications*. John Wiley & Sons. ISBN: 9781119004134(p), 9781119004172(e).

Chang, S.S.L., & Zadeh, L.A. (1996). On fuzzy mapping and control. *IEEE Transactions on Systems, Man, and Cybernetics, SMC-2*(1), 30-34. https://doi.org/10.1109/TSMC.1972.5408553.

Duan, J.S., Rach, R., Baleanu, D., & Wazwaz, A.M. (2012). A review of the Adomian decomposition method and its applications to fractional differential equations. *Communications in Fractional Calculus*, *3*(2), 73-99.

Dubois, D., & Prade, H. (1982). Towards fuzzy differential calculus part 3: differentiation. *Fuzzy Sets and Systems*, *8*(3), 225-233. https://doi.org/10.1016/S0165-0114(82)80001-8.

Dumbser, M., Busto, S., Vázquez-Cendón, M.E., & Peshkov, I. (2023). Preface for the special issue “hyperbolic PDE in computational physics: advanced mathematical models and structure-preserving numerics”. *Applied Mathematics and Computation*, *450*, 127994. https://doi.org/10.1016/j.amc.2023.127994.

El Mfadel, A., Melliani, S., & Elomari, M.H. (2021). A note on the stability analysis of fuzzy nonlinear fractional differential equations involving the Caputo fractional derivative. *International Journal of Mathematics and Mathematical Sciences*, *2021*(1), 1-6. https://doi.org/10.1155/2021/7488524.

Eslami, M., & Rezazadeh, H. (2016). The first integral method for Wu–Zhang system with conformable time-fractional derivative. *Calcolo*, *53*(3), 475-485. https://doi.org/10.1007/s10092-015-0158-8.

Ganji, D.D. (2012). A semi-Analytical technique for non-linear settling particle equation of Motion. *Journal of Hydro-Environment Research*, *6*(4), 323-327. https://doi.org/10.1016/j.jher.2012.04.002.

He, J.H. (1999). Homotopy perturbation technique. *Computer Methods in Applied Mechanics and Engineering*, *178*(3-4), 257-262. https://doi.org/10.1016/S0045-7825(99)00018-3.

He, J.H. (2005). Application of homotopy perturbation method to nonlinear wave equations. *Chaos, Solitons & Fractals*, *26*(3), 695-700. https://doi.org/10.1016/j.chaos.2005.03.006.

Hoa, N., Vu, H., & Duc, T.M. (2019). Fuzzy fractional differential equations under Caputo–Katugampola fractional derivative approach. *Fuzzy Sets and Systems*, *375*, 70-99. https://doi.org/10.1016/j.fss.2018.08.001.

İbiş, B., & Bayram, M. (2014). Approximate solution of time-fractional advection-dispersion equation via fractional variational iteration method. *The Scientific World Journal*, *2014*(1), 1-5. https://doi.org/10.1155/2014/769713.

Jahan, S., Yadav, P., Shah, K., & Abdeljawad, T. (2025). An efficient wavelet technique for solving variable-order fractional equations arising in contaminant transport through porous media. *Fractals*, 2540238. http://dx.doi.org/10.1142/S0218348X25402388.

Karniadakis, G.E., Hesthaven, J.S., & Podlubny, I. (2015). Special issue on "fractional PDEs: theory, numerics, and applications". *Journal of Computational Physics*, *293*, 1-3. https://doi.org/10.1016/j.jcp.2015.04.007.

Kashyap, M., Gupta, S., Arora, H.D., & Verma, A.K. (2025). Numerical analysis of nanoparticle diffusion: solving time-fractional Klein–gordon equations with the Laplace Homotopy perturbation method. In *Recent Developments in Fractional Calculus: Theory, Applications, and Numerical Simulations* (pp. 223-240). Springer Nature, Switzerland.

Kashyap, M., Singh, S.P., Gupta, S., & Mehta, P.L. (2023). Novel solution for time-fractional Klein-Gordon equation with different applications. *International Journal of Mathematical, Engineering and Management Sciences*, *8*(3), 537-546. https://doi.org/10.33889/IJMEMS.2023.8.3.030.

Keshavarz, M., Qahremani, E., & Allahviranloo, T. (2022). Solving a fuzzy fractional diffusion model for cancer tumor by using fuzzy transforms. *Fuzzy Sets and Systems*, *443*(part A), 198-220. https://doi.org/1/10.1016/j.fss.2021.10.009.

Kirtiwant, P.G., Khan, F., & Khan, A.A. (2017). Solution of FPDE in fluid mechanics by ADM, VIM and NIM. *American Journal of Mathematical and Computer Modelling*, *2*(1), 13-23. https://doi.org/10.11648/j.ajmcm.20170201.13.

Kumar, D., Agarwal, R.P., & Singh, J. (2018). A modified numerical scheme and convergence analysis for fractional model of Lienard's equation. *Journal of Computational and Applied Mathematics, 339*, 405-413. https://doi.org/10.1016/j.cam.2017.03.011.

Kumar, K., Pandey, R.K., & Sharma, S. (2017). Comparative study of three numerical schemes for fractional integro-differential equations. *Journal of Computational and Applied Mathematics*, *315*, 287-302.

Li, L., Jiang, Z., & Yin, Z. (2020). Compact finite-difference method for 2D time-fractional convection–diffusion equation of groundwater pollution problems. *Computational and Applied Mathematics*, *39,* 1-34. https://doi.org/10.1007/s40314-020-01169-9.

Li, Y., Zhang, Y., Chen, Y., & Chen, J. (2019). A fuzzy finite element method for solving fuzzy time-fractional advection–diffusion equations. *Journal of Computational Physics*, *390*, 1-18.

Naeem, M., Rezazadeh, H., Khammash, A.A., Shah, R., & Zaland, S. (2022). Analysis of the fuzzy fractional-order solitary wave solutions for the kdv equation in the sense of Caputo-Fabrizio derivative. *Journal of Mathematics*, *2022*(1), 3688916. https://doi.org/10.1155/2022/3688916.

Nikan, O., Machado, J.A.T., Golbabai, A., & Nikazad, T. (2020). Numerical approach for modeling fractal mobile/immobile transport model in porous and fractured media. *International Communications in Heat and Mass Transfer*, *111*, 104443. https://doi.org/10.1016/j.icheatmasstransfer.2019.104443.

Pedro, F.S., Lopes, M.M., Wasques, V.F., Esmi, E., & de Barros, L.C. (2023). Fuzzy fractional differential equations with interactive derivative. *Fuzzy Sets and Systems*, *467,* 108488. https://doi.org/10.1016/j.fss.2023.02.009.

Petrá, I. (2011). *Fractional-order nonlinear systems: modeling, analysis and simulation*. Springer, Heidelberg. ISBN: 9783642181009(p), 9783642181016(e).

Podlubny, I. (1998). *Fractional differential equations: an introduction to fractional derivatives, fractional differential equations, to methods of their solution and some of their applications.* Elsevier. ISBN: 9780080531984.

Rahaman, M.M., Takia, H., Hasan, M.K., Hossain, M.B., Mia, S., & Hossen, K. (2022). Application of advection diffusion equation for determination of contaminants in aqueous solution: a mathematical analysis. *Applied Mathematics and Physics*, *10*(1), 24-31. https://doi.org/10.12691/amp-10-1-2.

Rezazadeh, H. (2018). New solitons solutions of the complex Ginzburg-Landau equation with Kerr law nonlinearity. *Optik*, *167*, 218-227. https://doi.org/10.1016/j.ijleo.2018.04.026.

Rezazadeh, H., Kumar, D., Sulaiman, T.A., & Bulut, H. (2019). New complex hyperbolic and trigonometric solutions for the generalized conformable fractional gardner equation. *Modern Physics Letters B*, *33*(17), 1950196. https://doi.org/10.1142/S0217984919501963.

Rubbab, Q., Nazeer, M., Ahmad, F., Chu, Y.M., Khan, M.I., & Kadry, S. (2021). Numerical simulation of advection–diffusion equation with caputo-fabrizio time fractional derivative in cylindrical domains: applications of pseudo-spectral collocation method. *Alexandria Engineering Journal*, *60*(1), 1731-1738. https://doi.org/10.1016/j.aej.2020.11.022.

Salahshour, S., Allahviranloo, T., & Abbasbandy, S. (2012a). Solving fuzzy fractional differential equations by fuzzy Laplace transforms. *Communications in Nonlinear Science and Numerical Simulation*, *17*(3), 1372-1381. https://doi.org/10.1016/j.cnsns.2011.07.005.

Salahshour, S., Allahviranloo, T., Abbasbandy, S., & Baleanu, D. (2012b). Existence and uniqueness results for fractional differential equations with uncertainty. *Advances in Difference Equations*, *2012*(1), 112.

Shah, F.A., Kamran, Boulila, W., Koubaa, A., & Mlaiki, N. (2023). Numerical solution of advection–diffusion equation of fractional order using Chebyshev collocation method. *Fractal and Fractional*, *7*(10), 762. https://doi.org/10.3390/fractalfract7100762.

Shah, K., Rehman, K.U., Abdalla, B., Abdeljawad, T., & Shatanawi, W. (2025). Using neural network and fractals fractional analysis to predict the eye disease infection caused by conjunctivitis virus. *Fractals*, 2540204. https://doi.org/10.1142/s0218348x25402042.

Shah, K., Seadawy, A.R., & Arfan, M. (2020). Evaluation of one dimensional fuzzy fractional partial differential equations. *Alexandria Engineering Journal*, *59*(5), 3347-3353. https://doi.org/10.1016/j.aej.2020.05.003.

Shah, S.A., Rehman, N., Ahmad, S., Elaffendi, M.A., & Ateya, A.A. (2025). Fractional discrete modeling and numerical analysis of hepatitis B and C dynamics with neural network approximation. *European Journal of Pure and Applied Mathematics*, *18*(3), 6481-6481. https://doi.org/10.29020/nybg.ejpam.v18i3.6481.

Singh, A., Das, S., Ong, S.H., & Jafari, H. (2019). Numerical solution of nonlinear reaction–advection–diffusion equation. *Journal of Computational and Nonlinear Dynamics*, *14*(4), 041003. https://doi.org/10.1115/1.4042687.

Singh, H. (2022). Jacobi collocation method for the fractional advection-dispersion equation arising in porous media. *Numerical Methods for Partial Differential Equations*, *38*(3), 636-653. https://doi.org//10.1002/num.22674.

Tapaswini, S., & Chakraverty, S. (2013). Numerical solution of n-th order fuzzy linear differential equations by homotopy perturbation method. *International Journal of Computer Applications*, *64*(6), 5-10. https://doi.org/10.5120/10636-5376.

Verma, L., Meher, R., Avazzadeh, Z., & Nikan, O. (2023). Solution for generalized fuzzy fractional Kortewege-de varies equation using a robust fuzzy double parametric approach. *Journal of Ocean Engineering and Science, 8*(6), 602-622. https://doi.org/10.1016/j.joes.2022.04.026.

Vu, H., Ghanbari, B., & Hoa, N.V. (2022). Fuzzy fractional differential equations with the generalized Atangana-Baleanu fractional derivative. *Fuzzy Sets and Systems*, *429*, 1-27. https://doi.org/10.1016/j.fss.2020.11.017.

Zadeh, L.A. (1965). Fuzzy sets. *Information and Control*, *8*(3), 338-353. https://doi.org/10.1016/S0019-9958(65)90241-X.

Zafar, Z.U.A., Sene, N., Rezazadeh, H., & Esfandian, N. (2022). Tangent nonlinear equation in context of fractal fractional operators with nonsingular kernel. *Mathematical Sciences*, *16*(2), 121-131. https://doi.org/10.1007/s40096-021-00403-7.

Zhang, Y., Wei, T., & Yan, X. (2022). Recovery of advection coefficient and fractional order in a time-fractional reaction–advection–diffusion-wave equation. *Journal of Computational and Applied Mathematics*, *411*, 114254. https://doi.org/10.1016/j.cam.2022.114254.

Zureigat, H., Ismail, A.I., & Sathasivam, S. (2021). Numerical solutions of fuzzy time fractional advection-diffusion equations in double parametric form of fuzzy number. *Mathematical Methods in the Applied Sciences*, *44*(10), 7956-7968. https://doi.org/10.1002/mma.5573.